AD-A082 232 ARIZONA UNIV TUCSON OPTICAL SCIENCES CENTER F/G 20/10
ELECTROMAGNETIC ANISOTROPY.(U)
DEC 79 P A FRANKEN, J G SMALL, E BOGATIN F49620-77-C-0021
UNCLASSIFIED AFOSR-TR-80-0221 NL

1 OF 1
AD
A082232

END
DATE
FILMED
4-80
DTIC

ELECTROMAGNETIC ANISOTROPY

P. A. Franken, J. G. Small, and E. Bogatin

Optical Sciences Center
University of Arizona
Tucson, Arizona 85721

28 December 1979

Final Report for Period October 1, 1976 - Sept. 30, 1979

F49620-77-C-0021

Prepared for
Air Force Office of Scientific Research
Bolling Air Force Base,
D.C. 20332

Unclassified

SECURITY CLASSIFICATION OF THIS PAGE (When Data Entered)

REPORT DOCUMENTATION PAGE	READ INSTRUCTIONS BEFORE COMPLETING FORM
1. REPORT NUMBER: AFOSR TR-80-0221	2. GOVT ACCESSION NO. / 3. RECIPIENT'S CATALOG NUMBER
4. TITLE (and Subtitle): Electromagnetic Anisotropy	5. TYPE OF REPORT & PERIOD COVERED: Final Report 10/01/76 - 9/30/79
	6. PERFORMING ORG. REPORT NUMBER
7. AUTHOR(s): Peter A. Franken, J.G. Small, E. Bogatin	8. CONTRACT OR GRANT NUMBER(s): F49620-77-C-0021
9. PERFORMING ORGANIZATION NAME AND ADDRESS: Optical Sciences Center, University of Arizona, Tucson, Arizona 85721	10. PROGRAM ELEMENT, PROJECT, TASK AREA & WORK UNIT NUMBERS: 61102F 2301/A1
11. CONTROLLING OFFICE NAME AND ADDRESS: Air Force Office of Scientific Research/NP, Bolling AFB, D.C. 20332	12. REPORT DATE: 28 December 1979
	13. NUMBER OF PAGES: 66
14. MONITORING AGENCY NAME & ADDRESS (if different from Controlling Office)	15. SECURITY CLASS. (of this report): Unclassified
	15a. DECLASSIFICATION/DOWNGRADING SCHEDULE

16. DISTRIBUTION STATEMENT (of this Report)

Approved for public release; distribution unlimited.

17. DISTRIBUTION STATEMENT (of the abstract entered in Block 20, if different from Report)

18. SUPPLEMENTARY NOTES

19. KEY WORDS (Continue on reverse side if necessary and identify by block number)

Anisotropy
Speed of light
Relativity
Absolute motion
Ether wind
Stabilized lasers
High-precision tests

20. ABSTRACT (Continue on reverse side if necessary and identify by block number)

Two new precision laser interferometric tests of the postulates of special relativity are described. Two independent frequency stablized lasers, situated on the circumference of a rotable platform beat together at the center. A variation in the beat frequency as the table rotates can be interpreted as a one way anisotropy in the speed of light. A test for a round trip anisotropy is made by monitoring the cavity length change as the laser orientation change. This can also be interpreted as a mass anisotropy in space.

DD FORM 1 JAN 73 1473 EDITION OF 1 NOV 65 IS OBSOLETE

Unclassified

SECURITY CLASSIFICATION OF THIS PAGE (When Data Entered)

TABLE OF CONTENTS

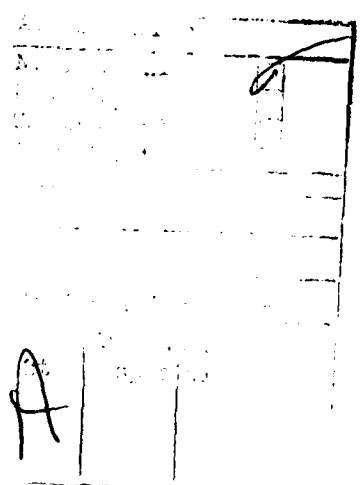

LIST OF ILLUSTRATIONS

LIST OF ILLUSTRATIONS--Continued

LIST OF ILLUSTRATIONS--Continued

SUMMARY

One hundred years ago Michelson began a search for a spatial dependence of the speed of light, motivated by the then current speculation of a luminiferous ether. Today, it is not necessary to invoke such an ether to justify a search for an optical anisotropy. With the discovery of the Rubin-Ford effect, and the cosmic blackbody radiation anisotropy, it is clear that the universe is not entirely isotropic or homogeneous and so it is plausible that there might be an anisotropy (likely minute) in the speed of light.

The experiment described here to test for a first order anisotropy consists of two independent laser oscillators situated on the circumference of a large rotatable platform. Their output beams are directed along radii to the center where they are interfered and their beat frequency is monitored. The relative propagation direction can be varied so as to test for any spherical harmonic of the anisotropy. (An antiparallel arrangement is sensitive to dipole distributions while an orthogonal alignment is sensitive to second harmonic or quadrupole distributions.)

As the table rotates, the beam directions move through space. An anisotropy in the speed of light will cause the phase of one beam at the center to shift relative to the other beam. This varying phase shift will cause a frequency modulation of the beat frequency at some harmonic of the table period. For a dipole anisotropy, the beat frequency variation has the same frequency as the table rotation. The detection of the magnitude and phase of this possible frequency variation would determine an anisotropy in the speed of light.

The assumption is made that the frequency of the laser oscillators is independent of their orientation. We use methane-stabilized He-Ne lasers to ensure good long-term frequency stability. Thus the output laser frequencies are tied to the rest frame frequencies of the methane molecule. There are three cosmological factors that might affect this postulated stability. An odd spatial harmonic in the light anisotropy will affect the Fabry-Perot cavity resonance to second order in v/c. An even harmonic will be effective to first order in v/c. A length strain in space might cause a cavity length strain, $\Delta L/L$, which then yields a frequency variation of $\Delta\nu/\nu = \Delta L/L$. Finally, a mass anisotropy might cause a variation of the transition frequency of the methane molecule depending on the induced dipole's direction.

To detect all of these possibilities we intend to monitor the feedback voltage which servoes the cavity length to match the Fabry-Perot resonance and the methane transition. By varying the polarization axis of the lasers we can search for mass anisotropy. Knowing the limit set by our first experiment on the speed of light anisotropy, a reasonable interpretation of the cavity length variation can be made.

The stabilized lasers and the rotating table represent the major components of this experiment. Two years of preliminary work have allowed us to pinpoint the weak points of the apparatus. The lasers' frequency stability was excessively worse than expected, primarily due to the low power of the lasers coupled with effects due to noisy detectors. New detectors have been obtained and more efficient lasers are being constructed.

The strongest environmental effect that influences the laser frequency is the table acceleration, which causes periodic compressions and expansions

of the laser cavity. We have decreased the rim acceleration significantly, and have accelerometers that could be used to null out any remaining acceleration. By searching for sidereal variation, not tied to the laboratory, we will be even less sensitive to these acceleration effects.

The results of the improved technology, augmented by the experience gained from our preliminary work, lead us to expect an ultimate sensitivity of $v/c < 10^{-10}$ for the odd and even spherical harmonic distribution of an anisotropy in the speed of light. We expect the second order experiment to yield a $(v/c)^2 = \Delta L/L = \Delta\nu/\nu < 4 \times 10^{-18}$.

INTRODUCTION

The first attempt at measuring an anisotropy in the speed of light is soon approaching its 100th anniversary. In 1881 Michelson[1] obtained an upper limit to the variation of the speed of light with direction of $(v/c)^2 \lesssim 10^{-8}$. All experiments since can be grouped into either second order experiments if they involve a round trip for the light path or first order if they involve only a one-way light path. The effect that is observed (a fringe shift, $\Delta\phi/\phi$, a frequency shift, $\Delta\nu/\nu$, a length change $\Delta L/L$, etc.) for second order experiments varies as $(v/c)^2$. For first order experiments, the effect goes as v/c. Since v/c is very probably small, first order experiments should be inherently more sensitive. Further, it may be possible to have a first order anisotropy but the second order effect might not exist.

Michelson and his followers were motivated from theoretical grounds that there might be an anisotropy to the speed of light due to an "ether." In recent years there has appeared new experimental evidence of cosmological anisotropies that might couple to the speed of light. Rubin et al.,[2] in looking at the distribution of the number density and velocity of galaxies with radial velocities from 3500 km/sec to 6500 km/sec have noticed a nonuniform distribution. Their data are consistent with a motion of the sun with respect to the local distribution of galaxies at 600 km/sec toward the Virgo Cluster.

The infrared observations by Smoot et al.,[3] of the cosmic microwave background radiation also suggest an anisotropy in color. They interpret

this to be a motion of our sun with respect to the primordial explosion and expanding coordinate system. One of the fundamental assumptions of cosmology, that of the homogeneity and isotropy of the universe, is violated experimentally. It is not unreasonable to expect other physical parameters that might be tied to the expanding primordial reference frame or the local mass rest frame to also show an anisotropy. Searches for such an anisotropy in the inertial mass of an electron in lithium atoms by Hughes et al.[4] and Drever,[5] have failed to uncover any anisotropy at the $\Delta m/m \lesssim 5 \times 10^{-23}$ level. However, the interpretation of this experiment is questionable. Brillet and Hall[6] have placed an upper limit on the anisotropy of a reference length with orientation of $\Delta L/L \lesssim 10^{-15}$.

An experimental search for a first order anisotropy in the speed of light[7] is described. In addition, we also discuss an on-going second order search for a speed of light anisotropy that can be interpreted as an anisotropy in the absorption frequency of the methane molecule. The following sections present the progress, status, and expectations for the two experiments. We summarize the near future goals in the conclusion.

THE ONE-WAY EXPERIMENT

The one-way experiment was first proposed by E. W. Silvertooth.[8] It consists of two independent laser oscillators whose output beams are directed at each other along radii of a rotatable platform (see Fig. 1).

If the lasers have nearly the same frequency, ν, then a superposition of the two light beams at the center, as shown, would produce a low frequency beat in a detector. Assume that the speed of light is $\vec{c} = c + \vec{v}$, where the anisotropy component along the light path is $v \cos\theta$ and where θ is the angle between the light beam from one laser and the preferred direction. If the frequencies of the two lasers are ν_1 and ν_2 then the

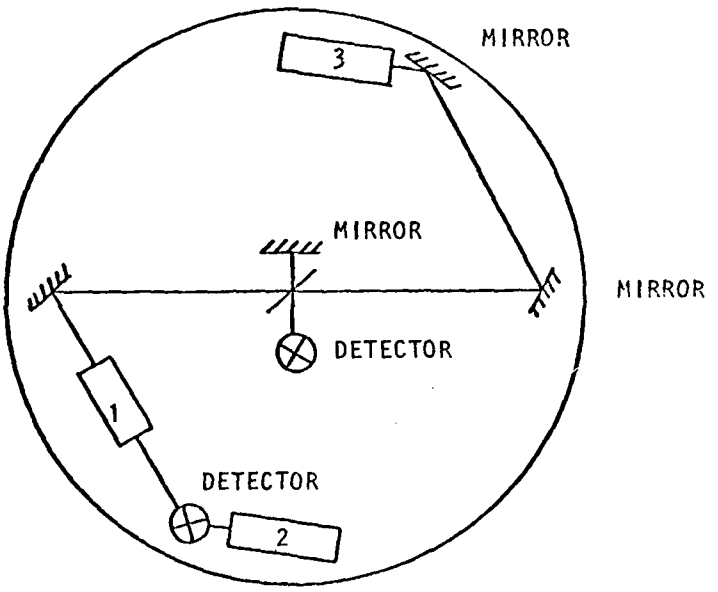

Fig. 1. Orientation of the three lasers on the rotating table. Lasers 2 and 3 are frequency stabilized. Laser 1 is offset stabilized to 2.

instantaneous relative phase, in cycles, at the center is

$$\phi_1 - \phi_2 = \nu_1 \left(\frac{L}{c + v\cos\theta} - t\right) - \nu_2\left(\frac{L}{c - v\cos\theta} - t\right) . \quad (1)$$

Expanding this to first order yields

$$\phi_1 - \phi_2 = t(\nu_2 - \nu_1) + \frac{L}{c}(\nu_1 - \nu_2) - (\nu_2 + \nu_1)\frac{L}{c}\frac{v}{c}\cos\theta. \quad (2)$$

When the platform is stationary, the beat frequency seen at the center is

$$\nu_{beat} = \frac{d}{dt}(\phi_1 - \phi_2) = \nu_2 - \nu_1 \quad (3)$$

assuming the laser frequencies to be constant. When the table rotates, an additional term is added and

$$\nu_{beat} = \frac{d}{dt}(\phi_1 - \phi_2) = (\nu_2 - \nu_1) + (\nu_2 + \nu_1)\frac{L}{c}\frac{v}{c}\frac{2\pi}{T}\sin\theta \quad (4)$$

with T = rotation period of the table.

We see that this beat will have a constant term $(\nu_2 - \nu_1)$ which may have some noise due to laser instability, and a term periodic with the table orientation. Since $\nu_1 \simeq \nu_2 = \nu$, then the periodic term is

$$\nu_{periodic} = \frac{4\pi}{T}\frac{L}{\lambda}\frac{v}{c}\sin\theta. \quad (5)$$

The maximum frequency excursion we expect for a $v/c = 10^{-4}$, the earth's orbital velocity about the sun, and a rotation period of 1 sec, is

$$\nu = \frac{4\pi}{T}\frac{L}{\lambda}\frac{v}{c} = 370 \text{ Hz}$$

where

L = 100 cm

$\nu = 3.39 \times 10^{-4}$ cm

$v/c = 10^{-4}$

T = 1 sec.

In general,

$$\frac{v}{c} = 2.7 \times 10^{-7} \nu_{period} \times T. \quad (6)$$

The frequency-stable lasers (Fig. 2) are locked to the inverse Lamb dip of methane in a He-Ne laser. A third laser is locked to one of the methane-stabilized lasers with a 5 MHz offset. This is to prevent injection locking or other coupling between the stabilized lasers. The stabilities of the lasers can be measured by observing the beat between any two lasers (see Fig. 3).

The beams traveling in opposite directions from the offset laser and the other methane stabilized laser are combined at the center of the table. This beat frequency is taken off the table by means of mercury slip rings and is measured with an HP 5345A frequency counter and recorded by a DIGITAL PDP-11 minicomputer. We search for a variation of this beat frequency with table orientation.

This is a dynamic measurement in that the signal depends on the rotation period of the table. If the frequency noise is independent of table velocity, we expect the signal-to-noise ratio (SNR) for a fixed integration time to be proportional to $(1/T)^{3/2}$. Our present upper limit on the first order anisotropy of the speed of light is $v/c \lesssim 6 \times 10^{-3}$, as seen in Fig. 4. The previous experimental problems that set this limit were:

--Rotation instabilities that limited the angular velocity and total integration time.

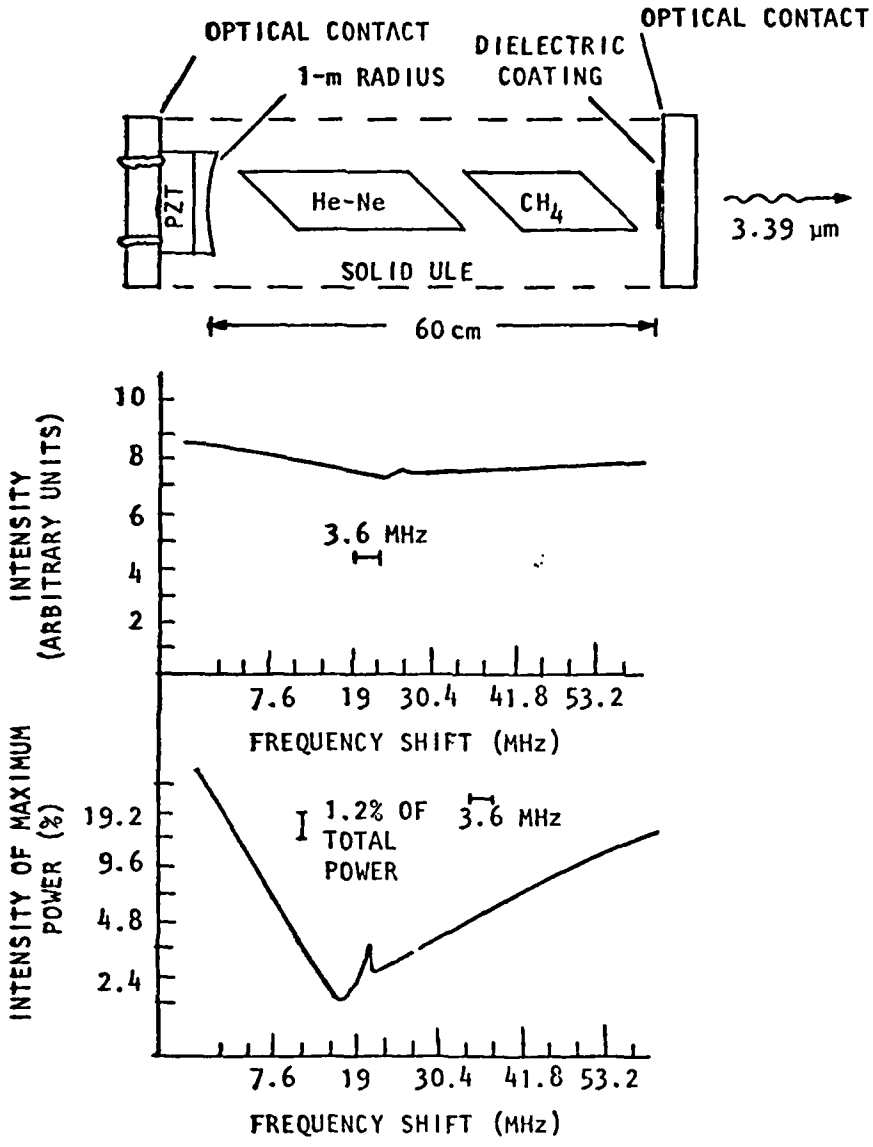

Fig. 2. Internal structure of the methane stabilized laser (top). Power out as the cavity length is increased (center). Power out vs frequency on an expanded scale showing the sharp maximum of the inverse Lamb dip with a width of ∿1 MHz FWHM (bottom).

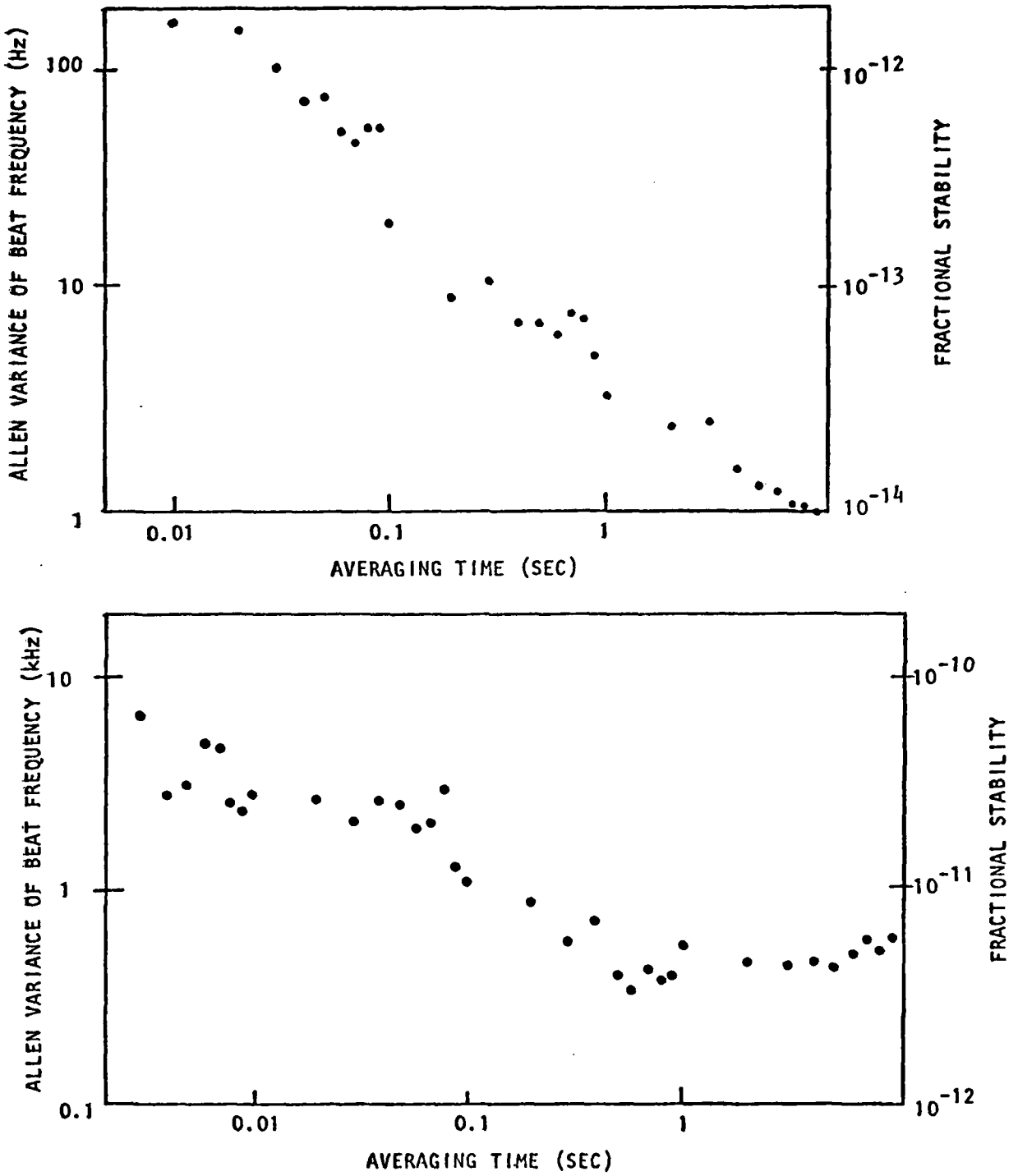

Fig. 3. Allan variance for the frequency variation of the offset beat frequency (top). Variance for the beat frequency between the offset laser and the other stabilized laser (bottom).

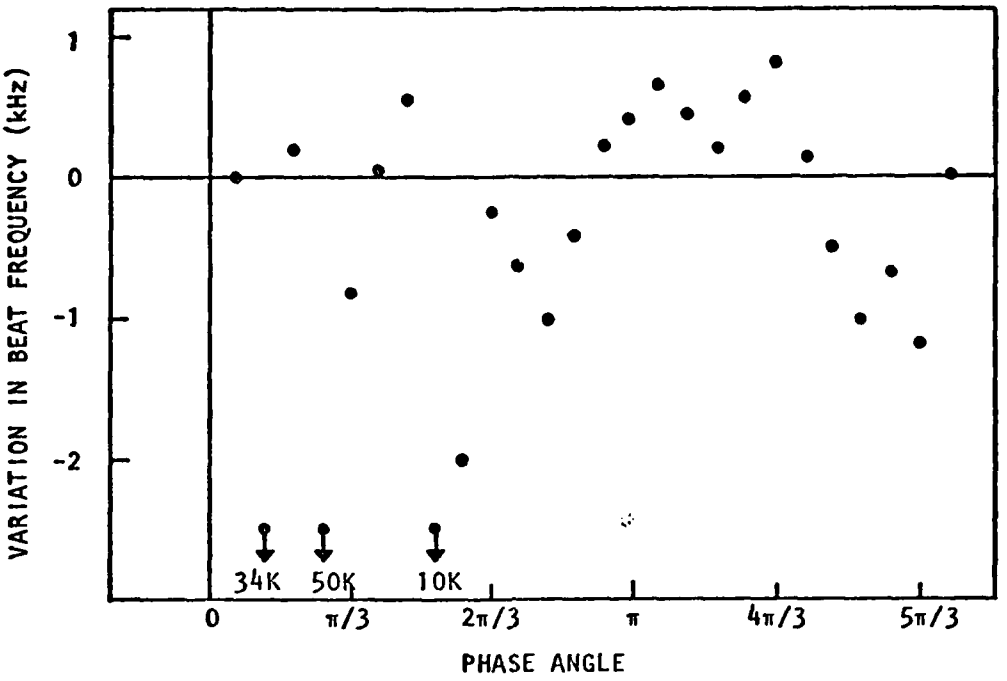

Fig. 4. Variation in the beat frequency between the offset and the other stabilized laser as the table rotates slowly. The graph represents 25 rotations that are averaged together and folded with the same phase. Note the effect of the vibration.

--High frequency mechanical vibrations of the table that caused laser frequency noise.

--A transient vibration as the table rotated.

--Inherent low frequency stability of the lasers.

In the following sections we describe these problems and how they have been overcome.

ROTATION INSTABILITY

The thrust air bearing built by the OSC shop supports the table in the vertical direction, but provides minimal radial stability with its 5^{o} cone shape. It does not take much perturbation to cause a radial instability where the table rocks about the central shaft. With the new model 4R journal bearing from Professional Instruments Co. and recently mounted to the rotating table by the OSC machine shop, this instability is removed. We have since rotated the table at speeds up to 0.3 Hz. This limit was set only because much of the electronics and lasers were not tied down well enough to withstand the almost 1 g centrifugal forces. In general, the acceleration at the rim is

$$a = 4 \times F^2 \tag{7}$$

where F is the table frequency in hertz and a is the rim centrifugal acceleration in g's.

At our expected operating rotation frequency of 1 Hz, there will be 4 g's at the rim. We have considered this in the design of the laser and electronics mounts and are currently making these final adjustments to allow such high rotation rates.

MECHANICAL VIBRATION OF THE TABLE

The most prominent source of laser frequency noise stems from the table vibration. By keeping the laser frequency stable to one part in 10^{11}, we are also keeping the cavity length stable to one part in 10^{11}. With a cavity length of 60 cm, this implies that length fluctuations are kept down to ± 0.06 A. We believe these vibrations are merely normal modes of the table being driven from various sources. Using the piezoelectric element from a crystal microphone and a HP302A wave analyzer we are able to record a scanning audio frequency spectrum of the mechanical vibration of the table. The one disadvantage of this system is that for reproducible results, we require the amplitudes of the Fourier components to be constant during the 5 minute scan time. This is not always the case.

Overhead mercury high intensity lights increase the amplitude noise less than 10% from that of a very quiet room. We show in Fig. 5 the vibration spectrum of the table with the room very quiet and no air flowing to the table but the lights on. We note very strong peaks at 120 to 180 Hz. With the hum of the air conditioners on, the vibration spectrum increases by over a factor of 5 in amplitude, as seen in Fig. 6. Figure 7 shows the higher frequency spectrum on a greatly expanded scale. Noise greater than 700 Hz clearly falls off rapidly probably with 1/f.

Even with the air conditioning off, when the table floats on air with 18 psi line pressure, the noise increases over an order of magnitude from the no-air case. The prominent noise peak is still $\sim$150 Hz as seen in Fig. 8. All the noise seems to cut off at 1.9 kHz. Most if it cuts off before 600 Hz.

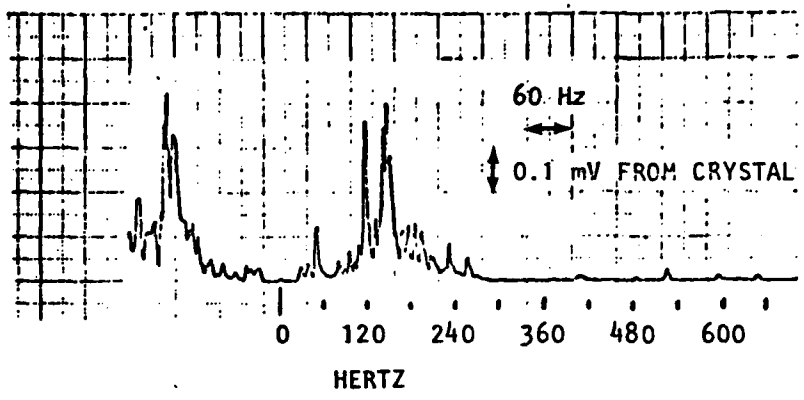

Fig. 5. Amplitude spectrum of vibration from the table with a 6 Hz bandwidth using a HP 302A wave analyzer. The scan rate was 20 Hz/sec. The scale is 0.1 mV from the crystal per centimeter. The room is very quite, no air is flowing to the table, and the air conditioner is off, but the overhead lights are on.

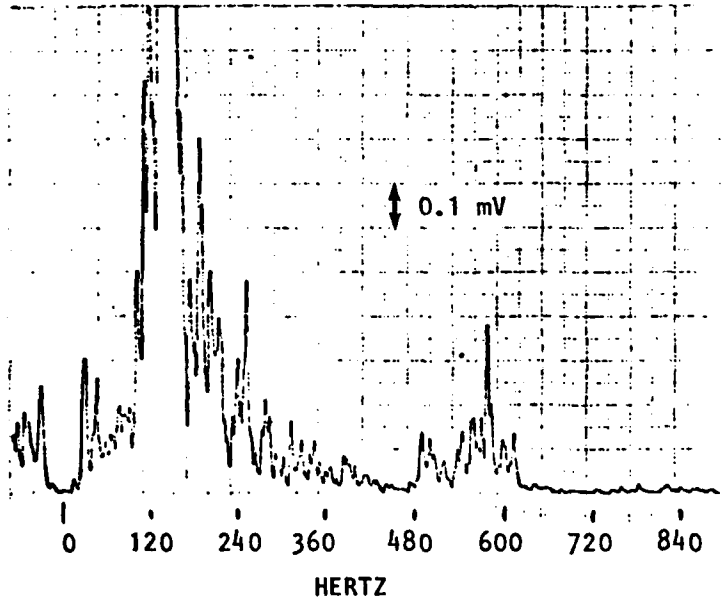

Fig. 6. Same situation as Fig. 5. No air to table, but with air conditioner on in the room. The scale is 0.1 mV from the crystal per centimeter.

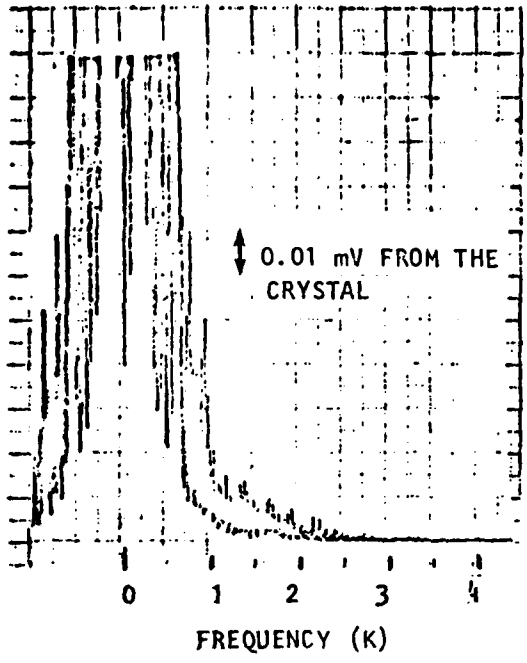

Fig. 7. Vibration spectrum with the air conditioner on, but no air to the table. The scan rate is 20 Hz/sec, but the vertical scale is 0.1 mV from the crystal per centimeter. Note the approximate 1/f falloff in amplitude, dropping away rapidly after ∿1 kHz.

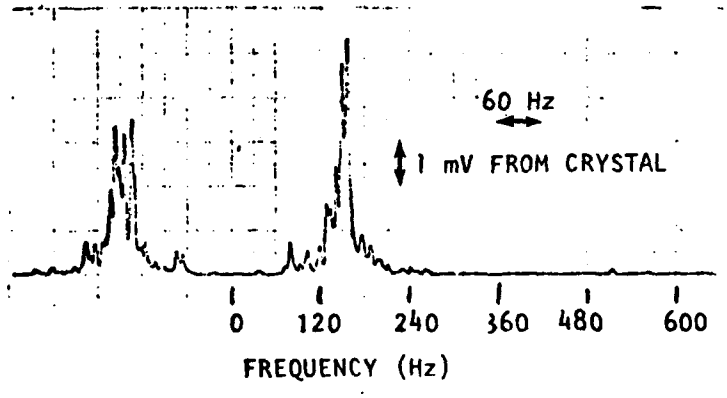

Fig. 8. Vibration spectrum with the air conditioner off, but table floating with 18 psi head pressure. Scan rate is still 20 Hz/sec, but the vertical scale is now 1 mV from crystal per centimeter. Compare this with Fig. 5, with no air flowing.

This behavior is not too unreasonable to expect. With no air, the table is in contact with the ground and normal mode vibrations are excited only by room acoustic noise and ground vibration noise. With air flowing, the table is freely supported and normal modes should not be as damped. Further, turbulence in the air flow will probably have an effect in exciting vibrations.

These spectra are very important in evaluating the necessary specifications of the laser servos. A minimum requirement is that they be faster than 200 Hz to minimize the effect due to the 150 Hz component. It is encouraging that there are very few higher frequency vibrations. Thus the servo properties are in reach and should be sufficient. It is not clear what the current frequency response limit is, but it seems to be ~100 Hz or less.

In addition to improving the active compensator, we are looking at more efficient passive mechanical isolators for mounting the lasers on the table. A 7L5 audio spectrum analyzer to aid in the vibration analysis is in the 1980 budget.

We have noticed that there is an optimum air line pressure of the thrust bearing to obtain lowest average noise. Figure 9 shows the noise amplitude with a 0.5 sec averaging vs the head pressure. It is clear than 30 psi is the best pressure to use. This, however, is for a floating, but not rotating, table. Similar measurements for a rotating table are in progress.

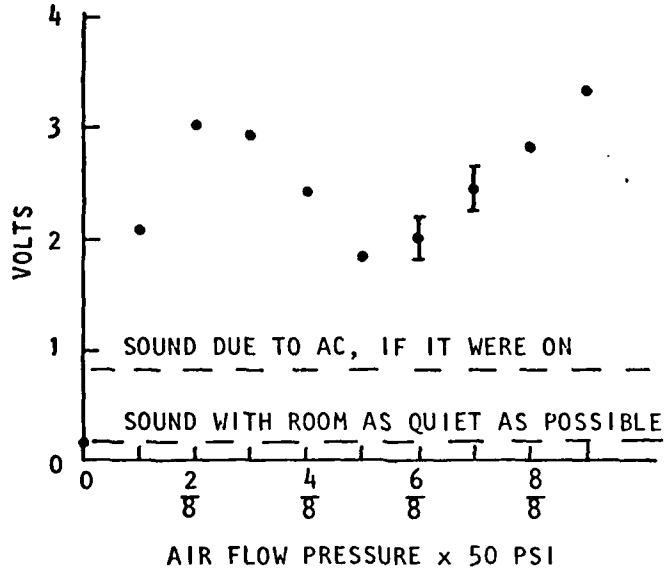

Fig. 9. Plot of the 0.5 sec averaged vibration amplitude on the table while it floats with no rotation vs the air flow head pressure. Note the clear minimum in the vibration noise with an air pressure of ∿35 psi. Superimposed is the background noise condition of a very quite room, and the sound due to just the air conditioning, showing the relative importance of these factors. No data are available on whether this minimum is present when the table rotates at constant velocity.

TRANSIENT VIBRATIONS

Within a period of 2 months, a bothersome bump appeared in the previously smooth rotation of the table. It occurred always when the table was in the same position and independent of the speed of rotation. It was also independent of whether the drive motor was connected. Observing the servo output of laser 3 in Fig. 10 makes it obvious that this vibration, just barely audible, was drastically affecting the laser stability.

We recorded the vibration amplitude vs orientation as the table rotated with a piezoelectric transducer on the table. The vibration effect is clear in Fig. 11. We varied the air pressure and hence air flow rate to look at its effect. There is some dependency, but the vibration never went away.

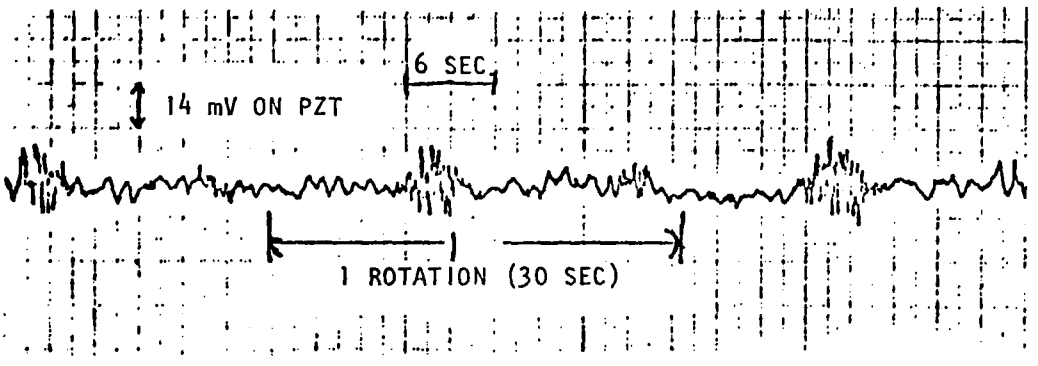

Fig. 10. Servo voltage onto the PZT of laser 3 as the table rotates with the old shaft in place. Clearly evident is the rapid compensation for the vibration.

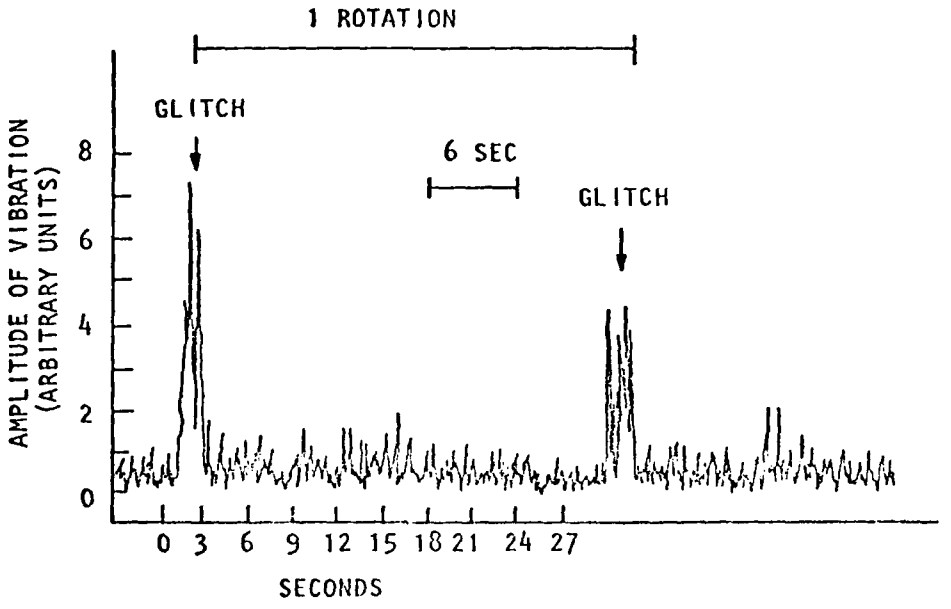

Fig. 11. Rectified amplitude of a crystal mike element in contact with the table. Extreme vibration occurs at one phase as the table rotates slowly.

After the rotating shaft was removed, a more sophisticated electronics arrangement was used to record the vibration. The AC signal from the crystal was amplified by 100 with a low noise circuit and then taken off the table. This AC signal was sent through a precision full-wave rectifier which was linear down to ±0.1 V input amplitude and probably lower. We were able to record the true averaged amplitude of the table vibration as it rotated. Figure 12 shows three rotations on an extended scale, with no obvious vibration apparent.

The clearance between the shaft and the hole through the stator of the bearing was very small. It is not hard to imagine that an imbalance of

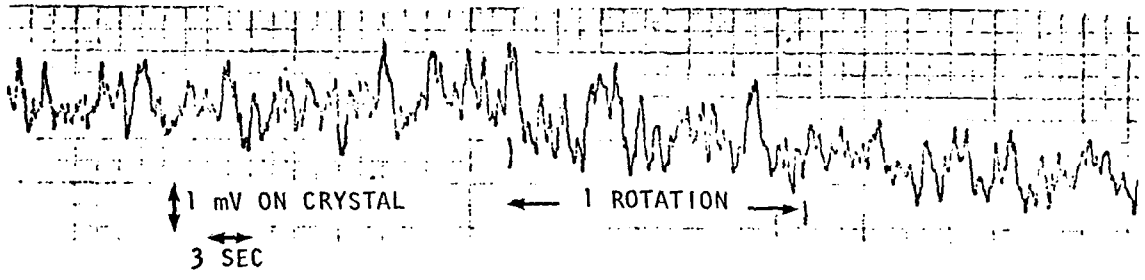

Fig. 12. Vibration amplitude of the table as it slows down freely. The period is ∿20 sec at this time. Three rotations are shown with no apparent vibration anomaly present.

the table caused a slight displacement of one side of the shaft which allowed two small protrusions to rub periodically causing the anomaly. With a new shaft designed with greater clearance and the new radial bearing there are no more obvious bumps present. The rotation is now very smooth.

INHERENT POOR FREQUENCY STABILITY OF THE STABILIZED LASERS

We offer two methods of estimating the frequency stability of the methane stabilized He-Ne lasers, if the limitation is set by the SNR of the detector that monitors the power in the beam.

If we assume the inverse Lamb dip peak has a Lorentzian profile, then the voltage out of the detector vs the detuning, ν, is given by

$$V_{out} = V_p \frac{\gamma^2}{\gamma^2 + \nu^2} \tag{8}$$

where

V_p = voltage out of detector at the peak

γ = half width half maximum (HWHM) of the peak

ν = detuning from line center.

If we sit on the side of the peak at $\nu = \gamma$, where the slope is maximum, given by

$$\frac{dV_{out}}{d\nu} = -2V_p \frac{\gamma^2 \nu}{(\gamma^2 + \nu^2)^2} \tag{9}$$

with $\nu = \gamma$ then

$$\frac{dV_{out}}{d\nu} = \frac{1}{2} \frac{V_p}{\gamma} . \tag{10}$$

For some detector noise level, V_n, in voltage space, there corresponds a noise in frequency space of

$$\Delta\nu = 2\gamma \frac{V_n}{V_p} \tag{11}$$

by setting $V_n = dV_{out}$. We thus might estimate the frequency noise due to detector noise, measured at the same bandwidth to be

$$\frac{\Delta\nu}{\gamma} = 2\frac{V_n}{V_p}. \tag{12}$$

Now consider the source of noise in a lock-in measurement. If we dither the mirror so that the detuning, ν, is of the form

$$\nu = \nu_0 + \delta\nu \sin\omega t \tag{13}$$

where

ν_0 = slowly varying average detuning from line center

ω = modulation angular frequency

$\delta\nu$ = modulation index of detuning

then, substituting this into Eq. (8) yields

$$V_{out} = V_p\gamma^2/(\gamma^2 + \nu_0^2 + 2\nu_0\delta\nu \sin\omega t + \delta\nu^2 \sin^2\omega t). \tag{14}$$

If the average detuning is near line center, as it should be if the stability is detector noise limited, then $\nu_0 << \gamma$.

Further, we can expand the $\sin^2(\omega t)$ term as

$$\delta\nu^2 \sin^2\omega t = \frac{1}{2}\delta\nu^2(1 + \sin 2\omega t). \tag{15}$$

If the bandpass filter after the detector does not pass the second harmonic, then this term may be cancelled out, and we are left with

$$V_{out} = V_p\gamma^2/(\gamma^2 + 2\nu_0\delta\nu \sin\omega t + \frac{1}{2}\delta\nu^2). \tag{16}$$

Taking the $2\nu_0\delta\nu \sin\omega t$ term as small, since $\gamma >> \nu_0$, we have

$$V_{out} = V_p\gamma^2/(\gamma^2 + \tfrac{1}{2}\delta\nu^2)\left[1 - 2\nu_0\delta\nu\ \sin\omega t/(\gamma^2 + \tfrac{1}{2}\delta\nu^2)\right]. \qquad (17)$$

Because of the bandpass filter, only the AC term is of interest, which is

$$V_{out} = V_p\gamma^2/(\gamma^2 + \tfrac{1}{2}\delta\nu^2)^2(2\nu_0\delta\nu\ \sin\omega t). \qquad (18)$$

To find the optimum modulation index for best SNR, we wish to maximize V_{out} with respect to $\delta\nu$

$$\frac{d}{d\delta\nu}V_{out} = \gamma^2/(\gamma^2 + \tfrac{1}{2}\delta\nu^2)^2(2\nu_0\ \sin\omega t)$$

$$- 2\delta\nu\gamma^2/(\gamma^2 + \tfrac{1}{2}\nu^2)^2(2\nu_0\delta\nu\ \sin\omega t). \qquad (19)$$

Setting this derivative to zero yields

$$\gamma^2 + \tfrac{1}{2}\delta\nu^2 = 2\delta\nu^2 \qquad (20)$$

and

$$\delta\nu = \left(\frac{2}{3}\right)^{1/2}\gamma = 0.82\ \gamma \qquad (21)$$

as the condition for best SNR. Substituting this result, Eq. (21), into Eq. (18) then yields

$$V_{out} = 0.92\ \frac{V_p}{\gamma}\nu_0\ \sin\omega t. \qquad (22)$$

The lock-in will take the phase of V_{out} and compare it to the phase of the reference oscillator. With a perfect phase detector, the noise limit on the error signal is reached when the amplitude of the V_{out} term is on the order of the noise which gets through the passband of the tuned amplifier. This occurs when ν_0 gets close to line center. Thus, the noise limited value of ν_0 is given by, setting $V_{out} = V_n$ and $0.93 = 1$,

$$\frac{\nu_0}{\gamma} = \frac{V_n}{V_p} . \tag{23}$$

We might expect that for one sweep of the dither, the frequency stability is given by Eq. (23). If the noise decreases with $1/\sqrt{n}$, where n is the number of sweeps, $n = 2\pi\omega\tau$, then

$$\frac{\nu_0}{\gamma} = \frac{V_n}{V_p} \frac{1}{(2\pi\omega\tau)^{\frac{1}{2}}} . \tag{24}$$

Currently, $2\pi\omega = 3$ kHz. Thus, we expect

$$\frac{\nu_0}{\gamma} = 2 \times 10^{-2} \frac{V_n}{V_p} \frac{1}{\sqrt{\tau}} . \tag{25}$$

We have measured γ to be 500 kHz. Thus,

$$\nu_0 = 10^4 \text{ Hz} \frac{V_n}{V_p} \frac{1}{\sqrt{\tau}} \tag{26}$$

where τ is in units of seconds.

It is our belief that the limitation of the frequency stability currently obtained with the methane stabilized lasers is due to the SNR of the detectors that sense the intensity variation with frequency dither. We have obtained a rough calibration of the power from laser 3 in normal operation using the circuit of Fig. 13 and an InAs photodiode. It is on the order of 15 μW. The peak height is from 2 to 4% of the full beam intensity. The ultimate limitation of the SNR is set by the shot noise in the detector. If we dither at a frequency f_d, then in a quarter of a period we will detect I_p $1/4f_d$ "photons." The Poisson noise for this intensity is

$$N = (I_p/4f_d)^{\frac{1}{2}}. \tag{27}$$

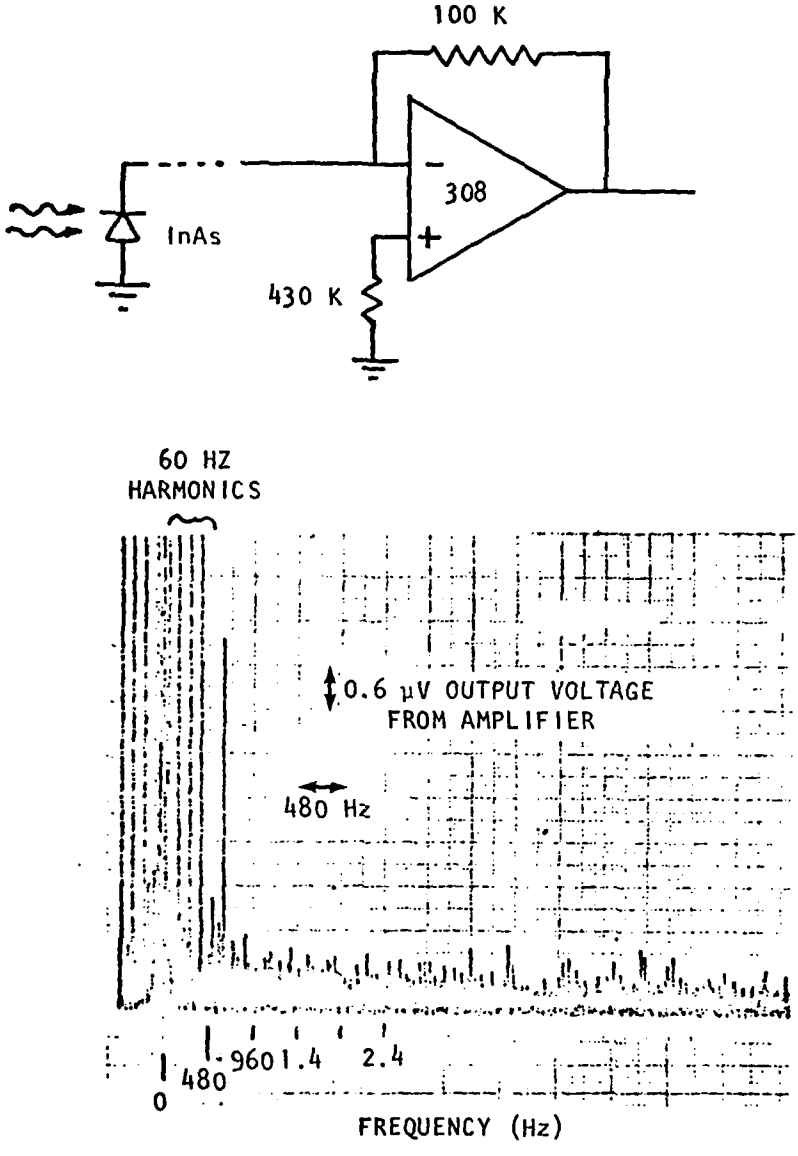

Fig. 13. Transconductance circuit used to monitor the photo current from the unbiased photodiode (top). The 430 k resistor shorting the noninversting input cancels the input offset voltage. The output noise spectrum from this circuit with the input floating (bottom). The 1/f noise cuts off at 200 Hz. The output noise, 1 μV, is for a 6 Hz bandwidth, so the input noise is $\sim 4 \times 10^{-13}$ A/$\sqrt{\text{Hz}}$.

The signal corresponds to a change of 2% of the full beam intensity in a time $1/4f_d$, so $S = 0.02\ I_p/4f_d$. Thus

$$SNR = 0.02\ (I_p/4f_d)^{\frac{1}{2}}. \tag{28}$$

Since $h\nu$ for 3.4 μm is 5.6×10^{-20} joules (0.35 eV) and $I = 15 \times 10^{-6}$ W, then $I_p = 2.6 \times 10^{14}$/sec. Taking $f_d = 3 \times 10^3$ Hz, then

$$SNR = 0.02 \left(\frac{2.6 \times 10^{14}}{12 \times 10^3}\right)^{\frac{1}{2}} = 2.8 \times 10^3. \tag{29}$$

From Eq. (26) we have the frequency noise ν_0

$$\nu_0 = 10^4 \text{ Hz } \frac{1}{\sqrt{\tau}} \frac{V_n}{V_p}. \tag{30}$$

Taking the shot noise limit

$$\frac{V_n}{V_p} = \frac{N}{S} = 3.5 \times 10^{-4} \tag{31}$$

and

$$\nu_0 = 10^4 \frac{1}{\sqrt{\tau}} 3.5 \times 10^{-4} = 3.5 \frac{1}{\sqrt{\tau}} \text{ Hz}. \tag{32}$$

We would thus expect ideal frequency stabilities of

3.5 Hz for 1 sec average

11 Hz for 0.1 sec average

35 Hz for 0.01 sec average

110 Hz for 0.001 sec average.

Our present detector is an InAs photodiode model J-12LD of Judson Research and Manufacturing Company. These diodes are used to sense both the rf beat signal and the 3 kHz audio signal. They have been used in the photovoltaic mode with no biasing for both applications. The audio amplifier had

a bandwidth of $\sim 10^4$ Hz, centered at 3 kHz. We have measured the current noise of the photodiode using the configuration of Fig. 13 and a HP 302A wave analyzer. It is clear from Fig. 14 that there is much 1/f noise. With the rated responsivity of 0.6 A/W as stated in the specifications, the noise at 3 kHz is 6.5×10^{-10} W/$\sqrt{\text{Hz}}$. Roy Gibbson of Judson IR Division,[9] mentioned that the rated D* for the model J-12 is similar to that of the J-12LD model. This D* would yield an NEP of 5×10^{-12} W/$\sqrt{\text{Hz}}$, two orders of magnitude lower than we measure. However, he pointed out that the J-12LD is specially designed for optimum performance at high frequency and that the low frequency behavior of the J-12LD could be as poor as we have measured.

We can perform a conversion from the responsivity in the current mode to voltage mode easily since a beam of 15 μW yields 10 μA in current mode and 0.5 mV in voltage mode (see Fig. 15 for clarification). Thus, the conversion is 2×10^{-2} A/V. With a rated responsivity of 0.6 A/W, this corresponds to 30 V/W. With a noise figure at 3 kHz of 6×10^{-10} W/$\sqrt{\text{Hz}}$, this corresponds to a voltage noise of 1.8×10^{-8} V/$\sqrt{\text{Hz}}$. The noise is thus 1.8×10^{-8} V/$\sqrt{\text{Hz}} \cdot (1 \times 10^4 \text{ Hz})^{\frac{1}{2}} = 2 \times 10^{-6}$ V. The typical signal for the peak height in voltaic mode for laser 3 is 20 μV (4% of the full intensity). This yields a SNR = 10. When viewing the power out of the laser as the cavity is tuned, this effect of poor SNR is masked by the noise of the 1A7A plug-in, being 10 μV for a 1 MHz bandwidth. Using Eq. (26), the expected frequency stability is given by

$$\nu_0 = 10^4 \text{ Hz} \frac{1}{\sqrt{\tau}} \frac{V_n}{V_p} = 10^4 \text{ Hz} \frac{1}{\sqrt{\tau}} \frac{1}{10} = 10^3 \text{ Hz} \frac{1}{\sqrt{\tau}} .$$

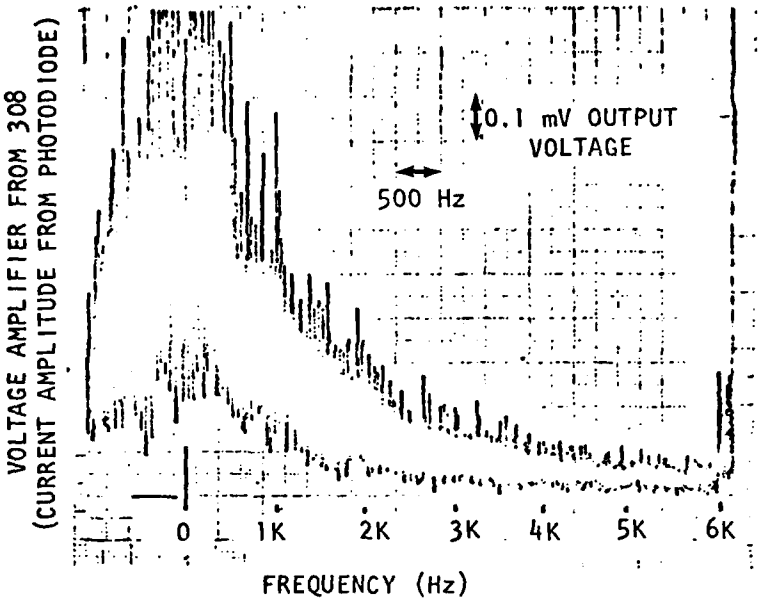

Fig. 14. Output noise from the circuit of Fig. 13 with the InAs detector connected at the input in a dark enclosure. At 3 kHz, the output noise is ∿0.1 mV or 10^{-9} A input current for 6 Hz bandwidth. This is 4×10^{-10} A/$\sqrt{\text{Hz}}$.

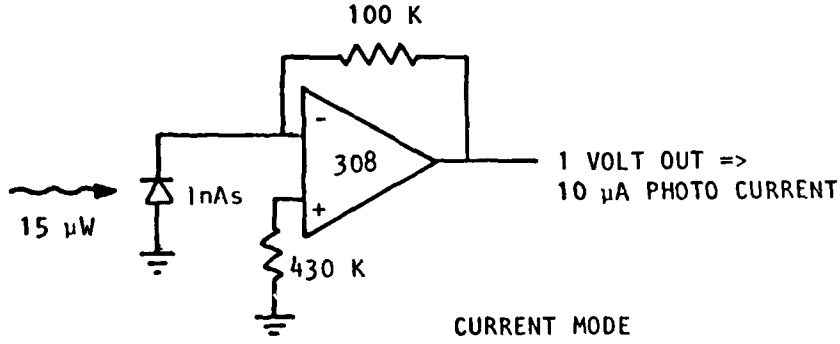

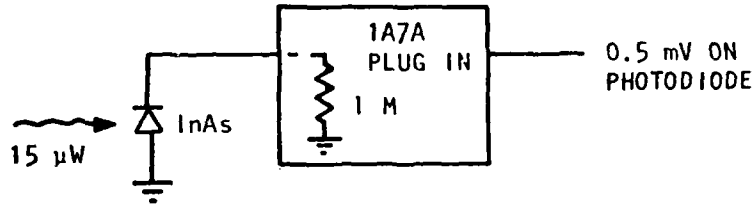

Fig. 15. Typical responses of the photodiode in current mode and voltage mode for the same incident power. The 15 μW calibration is from the rated responsivity in current mode.

This value is comparable to the observed value of 1 kHz beat stability between two lasers, as seen in Fig. 3.

The ultimate limitation of stability is set by the shot noise of the detector, being SNR = 2.8×10^3. We currently find SNR = 10.

The power of the beam is ~15 μW. If 2% of this is the signal, then $I_s = 3 \times 10^{-7}$ W. For a 1 kHz bandwidth, and SNR = 3×10^3, in order to be shot noise limited, the NEP of the detector should be

$$\text{NEP} = \frac{3 \times 10^{-7} \text{ W}/\sqrt{1 \text{ kHz}}}{3 \times 10^3} = 3.1 \times 10^{-12} \text{ W}/\sqrt{\text{Hz}} \qquad (33)$$

at 3 kHz. There are two obvious possibilities: either a cooled PbSe or an InAs detector.

A PbSe detector of Infra Red Industries model 5036, has an NEP of 3×10^{-11} W/$\sqrt{\text{Hz}}$ at 3 kHz at room temperature. The model 5637, a one-stage thermoelectrically cooled detector has an NEP of 1×10^{-11} W/$\sqrt{\text{Hz}}$ at 3 kHz. The model 5737, a two-stage cooled PbSe detector has an NEP of 6.6×10^{-12} W/$\sqrt{\text{Hz}}$.

The Judson IR model J-12 InAs photodiode is designed for optimum performance in the low modulation frequency range. A three-stage thermoelectrically cooled detector which requires only conduction heat sinking, has an NEP quoted by Roy Gibbson of 3×10^{-12} W/$\sqrt{\text{Hz}}$. Both of these compare favobrably with the required NEP of 3×10^{-12} W/$\sqrt{\text{Hz}}$.

We have purchased a two-stage thermoelectrically cooled InAs detector from Judson IR Industries. Preliminary work with it is very encouraging. There is a dramatic decrease in the noise as it is cooled from room temperature to -40°C. No special heat sinking is necessary as the power dissipation is only 1 W and the substrate has a large surface area. We are now

building special adapters to mount the detectors and their amplifier and special processing boxes on the table. The three additional detectors required are in the 1979-1980 budget.

Another possible remedy to increase the SNR is to increase the power out of the laser. The low output power of 15 μW is probably due to three mechanisms. The gain of the He-Ne laser is exponential with the length of the capillary discharge. The actual length is only 9 inches. With the absorption of the methane cell and other loss mechanisms, the short length may not be enough to raise the lasing medium much above threshold. We have redesigned the laser tube and methane absorption cell to allow twice as long a capillary tube length.

An obvious source of loss is absorption in the Brewster windows. In the gain tubes, we have switched to CaF_2 windows. However, the methane absorption cells still have 2 mm thick quartz windows. With the assistance of Drs. Mike Jacobson and Richard Lamoreaux of the solar energy materials measurement lab, a support facility of the Optical Sciences Center, we have measured the absorption spectra of the quartz windows. In comparing the absorption of a 2 mm window and 1 mm window in the two arms of a balanced IR spectrophotometer system, we eliminate the effects of dielectric surface reflection. A 1 mm thickness of quartz window has an absorption at 3.4 μm of ∿2%. A comparison of a 1 mm CaF_2 window and a 2 mm quartz window also shows about 2% absorption in the quartz as seen in Fig. 16. For the stabilized lasers, which have two 2-mm quartz windows, this corresponds to an additional 16% loss per round trip. The new laser tubes and absorption cells will all use CaF_2 windows.

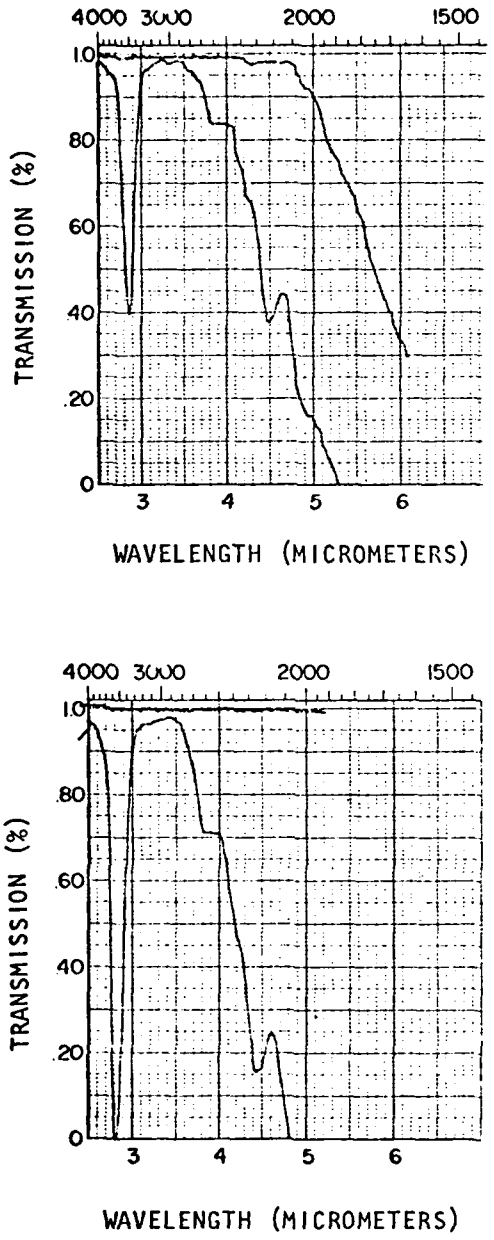

Fig. 16. Transmission spectra for a 2 mm thick quartz window compared with a 1 mm thick quartz window in the reference arm (top) and a 1 mm thick CaF_2 window in the reference arm. Both cases show about 2% absorption for one pass through the effective 1 mm thickness of the quartz window.

The laser cavity is formed by a flat dielectric coated mirror and a 1 m radius curved mirror separated by 60 cm. The beam waist will be at the flat mirror. The diameter of the waist is given by

$$\omega_0 = \omega_1 \left(\frac{L\lambda}{\pi}\right)^{\frac{1}{2}} \left(\frac{g_2}{g_1(1 - g_1 g_2)}\right)^{\frac{1}{4}} \tag{34}$$

with

$g_1 = 1 - 1/\infty$

$g_2 = 1 - 0.6/1 = 0.4$

$L = 60$ cm

$= 3.39 \times 10^{-4}$ cm

and

$\omega_0 = 8 \times 10^{-2}$ cm $\times$ 0.9 $= 7.2 \times 10^{-2}$ cm $= 0.72$ mm.

The spot size at the curved mirror is given by

$$\omega_2 = \left(\frac{L\lambda}{\pi}\right)^{\frac{1}{2}} \left(\frac{g_2}{g_2(1 - g_1 g_2)}\right)^{\frac{1}{4}} \tag{35}$$

$$= 8 \times 10^{-2} \times 1.4 = 1.1 \text{ mm.}$$

To allow the power leads of the gain cell easy access out of the ULE box, which spaces the mirrors, the gain cell is very near the curved mirror and hence the large spot size. This is awkward because the small capillary bore, which is 2.6 mm in diameter, is designed for a 0.72 mm spot size. With a larger spot size, there are much greater diffraction losses. Further, the absorption cell is very near the beam waist so that the transit time of a methane molecule in the beam is a minimum. This is the chief broadening mechanism for the inverse Lamb dip peak and limits the stability also. By

redesigning the other side of the box, we will be able to interchange the location of the gain cell and absorption cell, decreasing the diffraction loss and increasing the transit time of the methane in the beam, thereby gaining a bit in stability. Upon close observation of a laser tube, it was noticed that the capillary bore was not straight. There was as much as ±0.5 mm displacement of the axis from one end to the other. This makes the 2.6 mm bore effectively 2.1 mm, thereby increasing the loss. New tubes are being built by a glass blower at the Chemistry Department of the University of Arizona. By these actions, we expect to gain an order of magnitude increase in power out.

EXPECTATIONS FOR THE FIRST ORDER EXPERIMENT

We conservatively estimate that the stability will be 3.5 Hz for a 1 second average after the previously mentioned improvements are implemented. If the noise level is independent of rotation velocity, we might estimate an upper limit on the anisotropy in the speed of light to be

$$\frac{v}{c} \lesssim 10^{-6} = 2.7 \times 10^{-7} \times \nu_{noise} \times T$$

where ν_{noise} = 3.5 Hz and T = 1 sec, for one rotation of the table. If the noise is white, then the rms frequency noise amplitude should scale with $1/\sqrt{n}$, each average taking 1 sec. After 3 hours of averaging, we expect to have an upper limit of

$$\frac{v}{c} \lesssim 10^{-8}.$$

By searching for sideral periodicity, we might expect to gain another factor of 100 as Hall and Brillet do, to yield a final upper limit of

$$\frac{v}{c} \lesssim 10^{-10}.$$

SECOND ORDER SEARCH FOR AN ANISOTROPY IN THE SPEED OF LIGHT

In 1930 the limit of interferometric measurements of the speed of light anisotropy was reached by Joos[10] who measured an upper limit of $(v/c)^2 \lesssim 2 \times 10^{-11}$. A second generation of second order measurements was born in 1964 with the pioneering work of Jaseja et al.[11]

For a laser with cavity length L and anisotropy along the cavity axis of v cosθ, the output frequency is given by

$$\nu = q \frac{c}{2L}\left[1 - \left(\frac{v \cos\theta}{c}\right)^2\right] \tag{36}$$

where

q = a large integer

c = speed of light

ν = frequency of oscillation

v = anisotropy term in the speed of light

θ = angle between v and the cavity axis

The experiment of Jaseja et al. looked at the frequency variation of a He-Ne laser as it rotated, keeping L constant. They saw a 250 kHz variation which they attributed to magnetostriction of the Invar rods spacing the cavity. By looking for sideral variations they estimate an upper limit of 2 kHz due to an actual anisotropy effect. This sets their upper limit of $(v/c)^2 \lesssim 10^{-11}$.

Brillet and Hall[6] tried a clever variation. They stabilized the frequency of a He-Ne laser to the transmission fringe of a 10 cm long Fabry-Perot cavity which changed orientation. By comparing this frequency with a methane frequency stabilized He-Ne laser, they were able to set an upper limit on a length strain in space of $\Delta\ell/\ell \lesssim 10^{-15}$. More strictly, this experiment should be interpreted as only setting the limit for the difference in a speed of light and a length anisotropy.
limit for the difference in a speed of light and length anisotropy.

Our experiment is done along similar lines. The methane stabilized lasers are actively servoed so that their length, L, meets the condition

$$L = q \frac{c}{2\nu} \left[1 - \left(\frac{v \cos\theta}{c}\right)^2\right]. \tag{37}$$

We make the assumption that the center of the absorption frequency in the rest frame of the methane molecule is isotropic, i.e., independent of absorbed light direction. Thus, ν should be constant, independent of the orientation of the laser. As the laser rotates, to keep ν constant requires L to change, with

$$\Delta L = q \frac{c}{2\nu} \frac{v^2 \cos^2\theta}{c^2} \tag{38}$$

and

$$\frac{\Delta L_{max}}{L} = \left(\frac{v}{c}\right)^2. \tag{39}$$

We monitor this length change of the cavity by measuring the servo voltage on the PZT. With a sensitivity of 10^{-6} cm/V, we find

$$\left(\frac{v}{c}\right)^2 = \frac{\Delta L}{L} = 1.6 \times 10^{-11}\ \Delta V \tag{40}$$

with ΔV in millivolts. The system arrangement that allows us to monitor and record length changes as the cavity rotates is diagrammed in Fig. 17. It should be noted that because of the $\cos^2\theta$ term, the periodic length change due to an anisotropy of the speed of light is twice periodic with one table rotation. Using a computer buffer memory, we are able to average the PZT voltage of many rotations to remove the nonperiodic noise. In order to perform a fast Fourier transform (FFT) on the data, we record 9.1 rotations of the table in one buffer length. Each successive sweep is then added to the buffer and the buffer is finally divided by the total number of sweeps. A FFT of the buffer then yields information about signals once periodic with the table in harmonic 9 and signals twice periodic with the table rotation in harmonic 18. We show in Fig. 18 the buffer for one typical run containing the PZT servo voltage for 9.1 rotations of the table. We see that there is an obvious first-order component. The second-order component at harmonic 18 may be due to harmonics of whatever produces the first order signal rather than a true anisotropy in the speed of light. With a second harmonic amplitude of 0.8 mV, this corresponds to an effective $(v/c)^2 \leq (\Delta L/L) \approx 1.3 \times 10^{-11}$. All the data taken so far show a clear first-order signal of 1 to 2 mV with a second-order component of 0.5 to 1 mV. We believe this effect is due to the lasers reacting to the nonuniform rotation velocity of the table.

We have measured the cavity length response to an acceleration of the table by applying a repeatable table acceleration and monitoring the resulting PZT response with a digital lock-in technique to enhance the signal-to-noise ratio. Figure 19 shows the long-term velocity behavior of the table with its pulsed acceleration. Figure 20 shows the phase relationship of

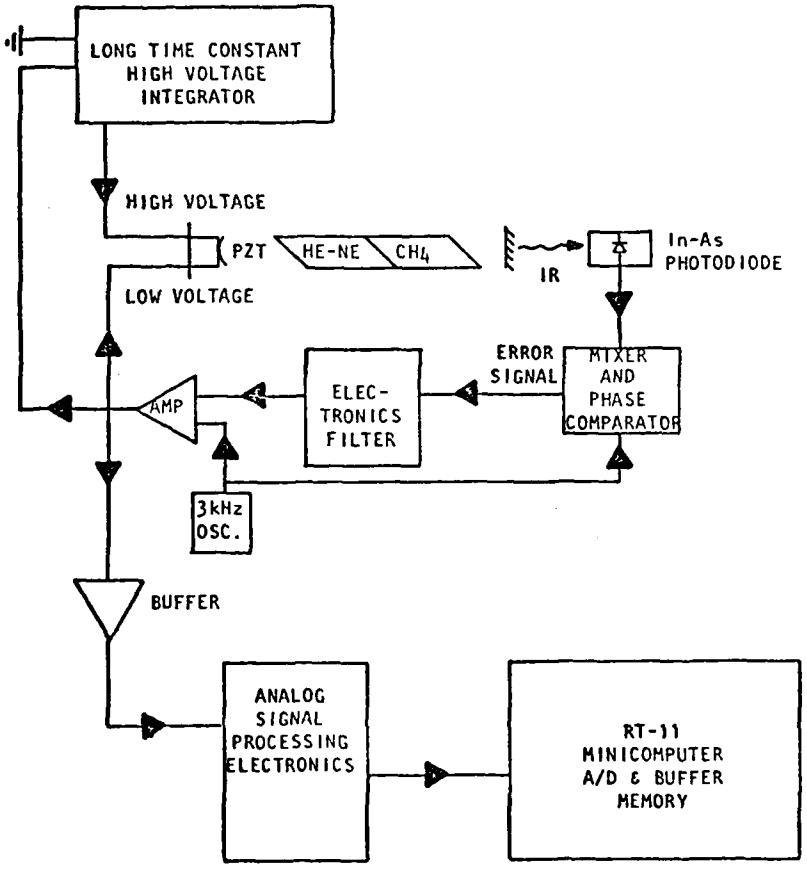

Fig. 17. Block diagram of the locking electronics and biasing techniques that allow monitoring of the low voltage PZT servo.

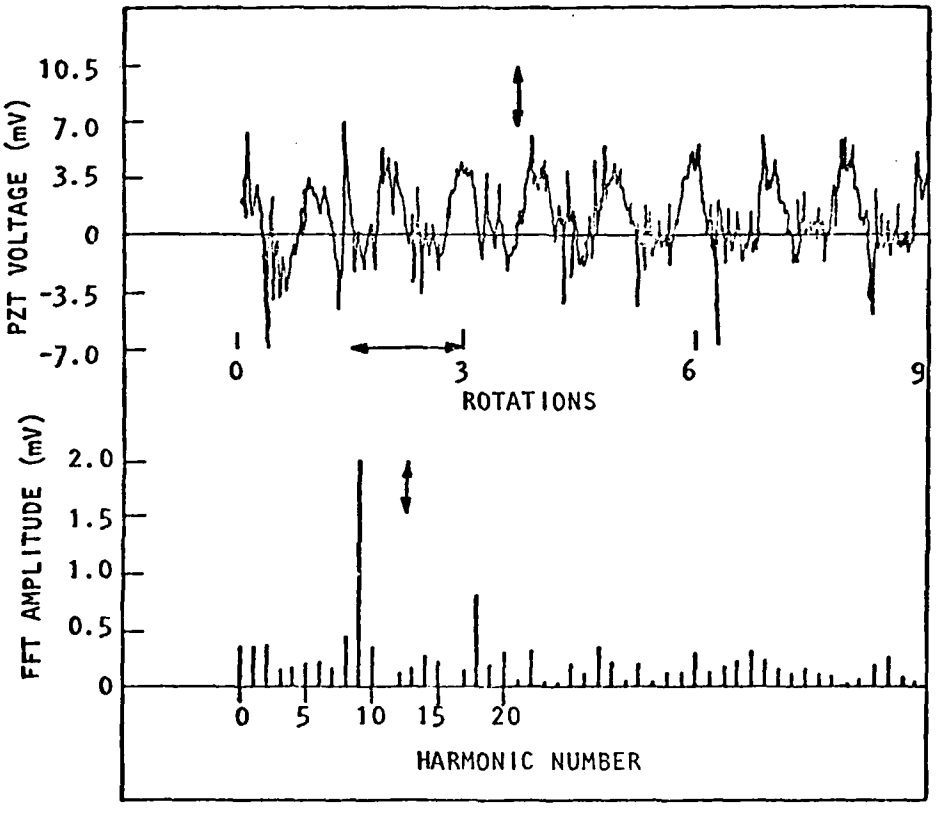

Fig. 18. PZT servo response of laser 3 as the table rotates at T = 28 sec. We have averaged 11 sweeps. Each sweep contains nine rotations of the table. Plotted blow is the first 50 harmonic amplitudes of the FFT spectrum for this buffer.

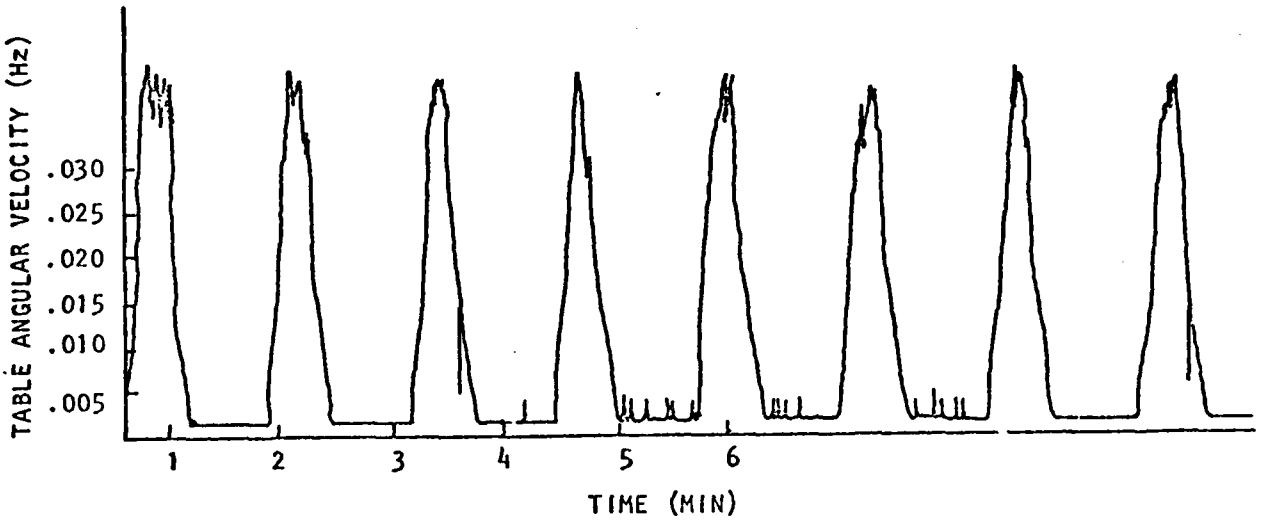

Fig. 19. Strip chart recording of the speed sensor frequency while the motor is driven by a triangular reference wave form of a 75 sec period. The maximum angular velocity of the table is 0.04 Hz. This corresponds to a period of 25 sec, comparable to our typical running velocity. Note that the table motion is relatively reproducible.

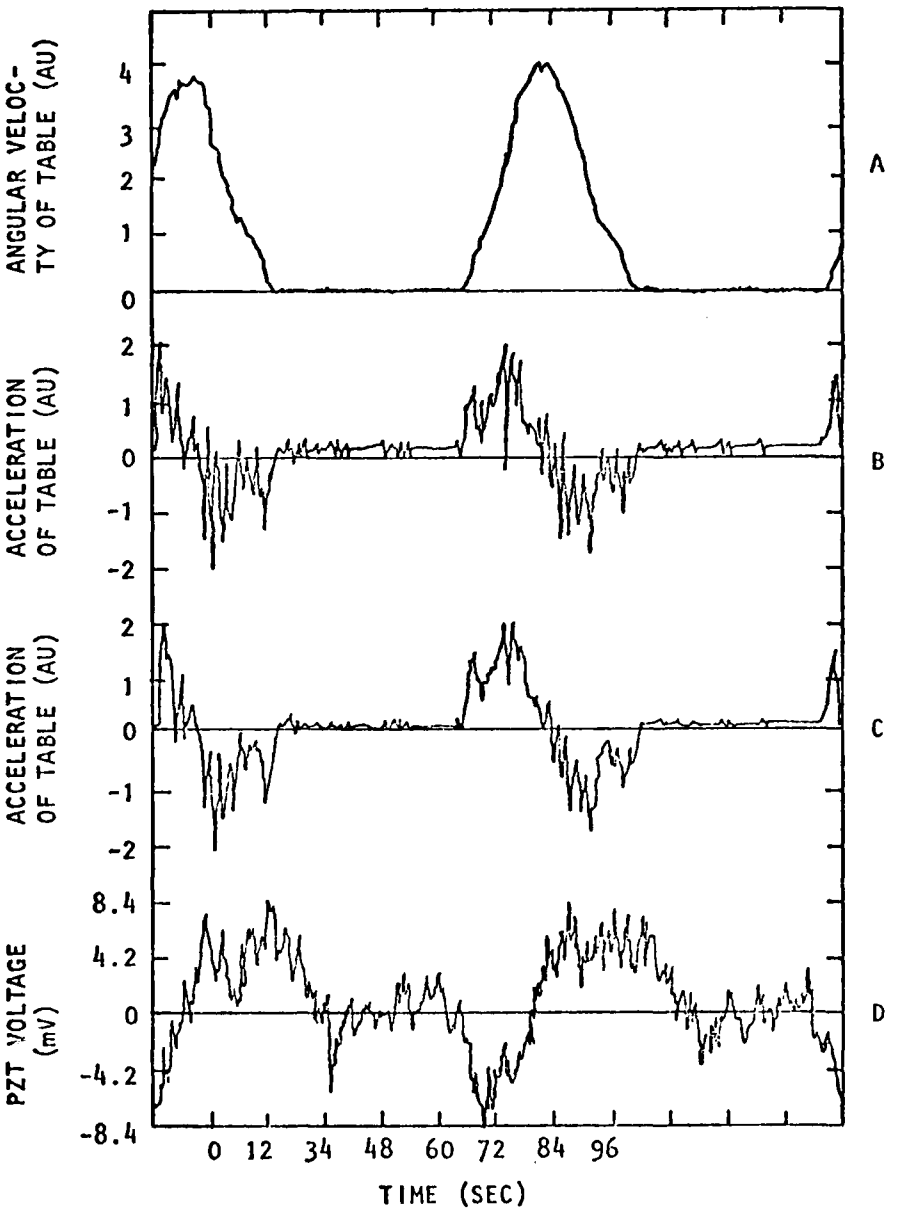

Fig. 20. Trace A is the angular velocity of the table. Traces B and C are numerical differentiations of this, yielding the table acceleration with 1 sec and 2 sec averaging, respectively. Trace D is the PZT response during this motion. A comparison of C and D shows the definite phase relation between the acceleration and the resulting PZT response.

the PZT response for the simultaneous angular velocity and acceleration of the table. We show 1.9 cycles of this pulsed behavior contained in the buffer. From this plot, it is obvious that the PZT responds to acceleration. We can estimate a $\delta L = 5.2 \times 10^{-9}$ cm length change in the cavity for an acceleration of the cavity of $a = 1.5$ cm/sec^2. A characteristic number of the PZT response is $\delta L/a = 3.5 \times 10^{-9}$ sec^2, or 3.5×10^{-6} cm/g.

One possible cause of this response may be that the acceleration produces a small pseudo-gravitational force that compresses the cavity slightly. The PZT response might be due to compensating for this length change. If one end of the cavity is effectively clamped, then the cavity will extend or compress depending on the direction of the acceleration, yielding the vector relation we see. To quantify this model we can imagine a rod supported from one end, being accelerated with a. A small section of length $d\ell'$, located ℓ' from the front, will have a strain given by $\delta d\ell'/d\ell' = P/E = \rho a\ell'/E$. Integrating we find the total length change

$$\delta L = \int_0^L \frac{\rho a \ell'}{E} \, d\ell' = \frac{\rho a L^2}{2E} \quad . \tag{41}$$

If we call $\rho = m/AL$, then

$$\delta L = maL/2AE. \tag{42}$$

Thus, this simple model predicts

$$\frac{\delta L}{a} = \frac{mL}{2AE} \, , \tag{43}$$

where

$m = 8.1$ kg

$L = 60$ cm

$A = 64$ cm^2

$E = 8 \times 10^{11}$ dyne/cm^2.

Then,

$$\frac{\delta L}{a} = 4.7 \times 10^{-9} \text{ sec}^2. \tag{44}$$

We see that the predicted number is within the 20% experimental limit of the measured value of $\delta L/a$, and we are not denied the elegance of the simple assumption. The fact that this model works so well suggests that the cavity is somehow clamped at one end. If it were held at both ends, one might expect to see a compression independent of the direction of acceleration. We see, however, compression and extension. One's physical intuition may not be reliable in this situation though, as we are dealing with length changes of only 0.5 Å.

This response is just what is required to account for the signals we have been seeing. The PZT response is 5.2 mV/1.5 cm/sec^2 = 3.5 mV/cm/sec^2. We note that at the frequency at which we typically take data, the table acceleration amplitude is 0.32 cm/sec^2. We would thus expect a PZT response of 1.1 mV amplitude. The typical amplitude we measure is from 1 to 2 mV. It is thus apparent that the stumbling block in our path to a smaller upper limit on $(v/c)^2$ is the acceleration of the table.

Using a value of $\delta\ell/a = 4 \times 10^{-9}$ sec^2, we have a sensitivity of 3.9×10^{-6} cm/g. This corresponds to 5.9 Hz/μg frequency shift at the rim. This effect is very critical in the second order experiment where one looks for compensation to the cavity length due to a second order anisotropy in

the speed of light. The table acceleration unfortunately also produces the exact same type of signal and ultimately sets the limitation to the second order limit of $(v/c)^2$. The first order experiment is not as sensitive to this effect since the PZT servo compensates for the length change always yielding nearly the same frequency output. However, there does seem to be some evidence of a periodic shift in the beat between the two stabilized lasers as the table rotates, which may be due to acceleration effects (see Fig. 21). This factor will certainly be investigated when the whole system is working. It is for these reasons that much effort has been spent in investigating the nature of the table acceleration.

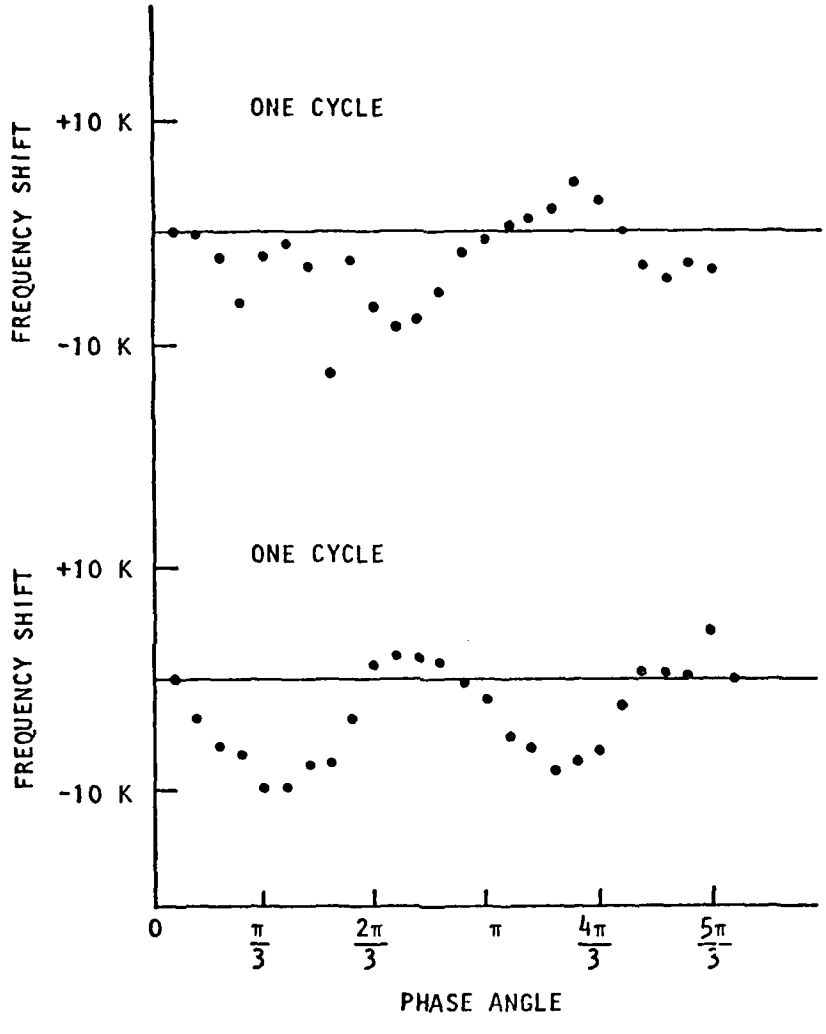

Fig. 21. Early data of the beat between the two lasers at the center of the table folded with the rotation of the table. Top and bottom plots are each one rotation spaced a few minutes apart. There is clearly some periodic behavior, whose origin is still uncertain but may be due to table acceleration.

TABLE ACCELERATION ANALYSIS

The rim acceleration of the rotating table can be reduced to 3 μg with a measurement noise level set by the statistics of the measurement process of ±2 μg. This is accomplished by careful dynamic weight balancing and judicious choice of the coupling "springs" from the driving motor to the table's shaft. We are currently working on the other important factor, which is table tilt. A further reduction of tilt will reduce the rim acceleration.

The Acceleration Measurement Process

If we limit attention to the first harmonic of the rim acceleration, we can describe the table frequency by

$$F = F_0 + \delta F \sin(2\pi F_0 t) \tag{45}$$

and

$$\alpha = \frac{dF}{dt} = 2\pi F_0 \delta F \cos(2\pi F_0 t) \tag{46}$$

where

F = instantaneous table speed

F_0 = average table speed

δF = modulation amplitude

α = rim acceleration.

Angular acceleration and all angular measurements are in cycles. The tangential acceleration is then

$$a = 2\pi\alpha R = 4\pi^2 F_0 \delta F \cos(2\pi F_0 t). \tag{47}$$

Looking at the magnitude only, we see that the rim acceleration in g's is given by

$$\frac{a}{g} = \frac{4\pi^2 R}{g} F\delta F \tag{48}$$

where R = 1 m, and

$$\frac{a}{g} = 4F_0\delta F \tag{49}$$

where F is in hertz. Calling $\beta = \delta F/F_0$, then

$$\frac{a}{g} = 4F_0{}^2\beta. \tag{50}$$

The Table Velocity Sensor

The problem of measuring the angular velocity of the table is a challenging physics question. What methods can be devised to measure the instantaneous angular velocity (within $\lesssim$ 0.1 sec) of the rotating table? Such possibilities as measuring the force on an adjacent magnet due to eddy current drag in the aluminum or measuring the Doppler shift of tangentially scattered laser light in a homodyne interferometer come to mind. Perhaps the frequency of a 1 kHz audio tone could be read from a magnetic recording tape wrapped on the rim.

Another possibility is optically detecting and measuring the time interval between equally spaced fiducial marks on the circumference of the table. The surface, which is accessible and closest to a circle, is the rotating air bearing itself. This is the most logical location for timing marks. There must be a minimum amount of jitter in the spacing of the marks and they must be closely spaced so as to provide the highest resolution possible. This can be achieved with a simple arrangement utilizing a strip

of 16-mm movie film that has sprocket holes spaced 4 mm apart. With 755 holes around the circumference of the rotating bearing (0.9 m diameter), there is a simple conversion from the pulse frequency of the speed sensor to the table frequency (table frequency = speed sensor frequency/755). This relationship has been confirmed experimentally to better than 0.5%.

An LED shines through the sprocket holes and is detected by a photo Darlington in a special mount. This detector is between the air bearing and the film. The film is spaced 6 mm from the air bearing with a few turns of UG 58 coaxial cable wrapped over the bearing and is uniformly positioned to within 1.6 mm. This sets the limitation in the speed-sensing stability due to phase noise in the triggering level. A layer of Teflon tubing is fitted over the detector so that the tape rides over this surface and is always in the same orientation. This prevents problems of tape flexing without rubbing and scratching of the detector surface. By carefully matching the ends of the 16-mm film that wraps around the rotating bearing, the joint glitch can be almost completely removed. There still remains a glitch corresponding to an advance of 15% of the phase at which the comparator triggers, occurring over 120 holes (16% of the circumference), and a small phase glitch at the joint due to the noncyclic match of the hole spacings and table circumference. Most of this might be removed by more careful alignment. This is the chief cause of the lower limit of the acceleration measurable.

At any selected position along the circumference a small wire can be placed which, while not affecting the speed sensor, will trigger a second optical gate that acts as a flag to set the rotation phase for computer analysis. A flip flop produces a frequency half that of the table. When

Q is low, the computer will accept table rotation speed data. When Q is high, the computer then does the numerical analysis. This always guarantees resetability to about 1 part in 1000, though it does mean that at best only every other revolution can be analyzed. This flag is completely decoupled from the sensor so that no half harmonics are present in the speed measurements.

To measure the f/v converter stability, a 100 Hz signal taken from a crystal, stable to one part in 10^8, acts as a reference. With the f/v converter using this signal, the effective table speed corresponds to 0.13 Hz, a factor of 2 of the typical frequency with which most of our data have been taken. We have used a Tektronix plug-in 7A22 as a preamplifier to provide gain and a DC offset to allow more easy determination of the stability of the f/v. This output signal was input via an A/D converter to a computer buffer of 1024 points at a sample rate of 0.2 Hz. A Fast Fourier transform was then done to provide the low frequency noise spectrum. Figure 22 shows the data in the buffer and the calculated spectrum on expanded scales. We note that at a frequency of 0.07 Hz and for a bandwidth of 1/512 (0.1 Hz), which is about the bandwidth in the measurement of the first harmonic of the table velocity, the voltage noise amplitude corresponds to $\beta = \Delta F/F \simeq 10^{-6}$. This may well be near the instrumental measuring limit in this setup, but offers a convenient upper limit to the fundamental f/v converter noise. At 0.07 Hz, this corresponds to

$$\left|\frac{a}{g}\right| = 4 \times (0.07\ \text{Hz})^2 \times 10^{-6} = 2 \times 10^{-8} \qquad (51)$$

f/v noise limit = 0.02 μg.

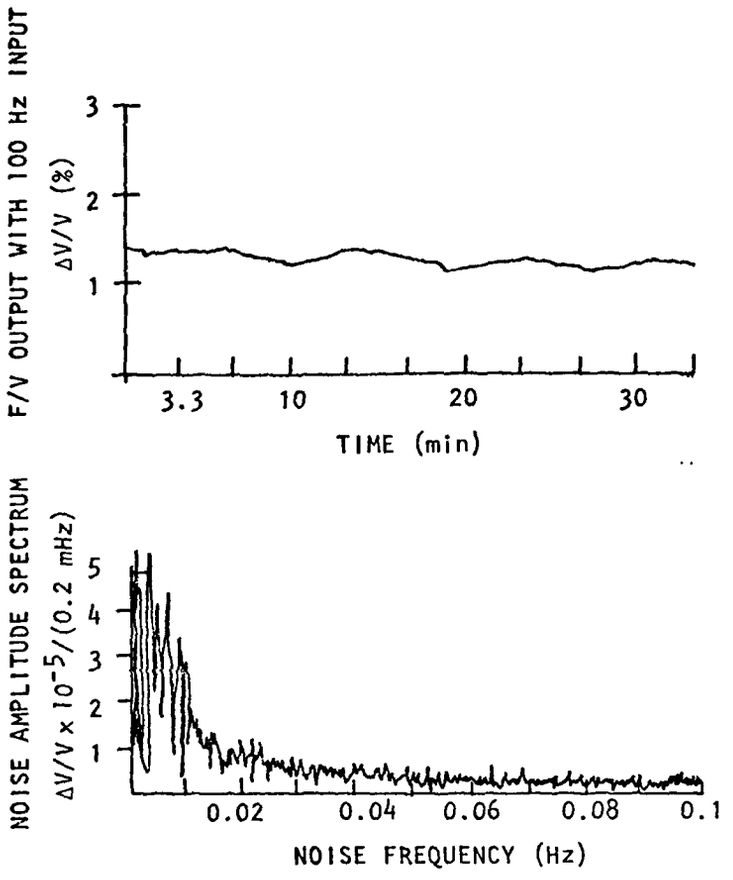

Fig. 22. f/v converter output with a 100 Hz stable reference frequency in. (Top) DC offset scale. The small apparent low frequency ripple is aliasing of the 0.2 Hz sample rate and the 100 Hz ripple. (Bottom) The FFT spectrum of the above data on an expanded scale. The amplitudes correspond to a bandwidth of 1/512 (0.1 Hz). The vertical scale is the noise voltage amplitude in parts per $10^5/(1/512 \times 0.1\ \text{Hz})$. The typical bandwidth of a measured first harmonic amplitude is $1/512 \times 0.07$ Hz.

A more immediate source of noise is due to the ripple of the integrated standard pulses. A large part of this has been filtered with an RC filter. However, there is a tradeoff. The larger the time constant, the less the ripple, but also the slower the time response. A sharper cutoff filter than an RC might be more appropriate. For these 14-sec-period rotations, we have used a 1-sec time constant, leaving a ripple effective noise of $\pm 2 \times 10^{-4}$ Hz. At slower speeds, the ripple is increased in amplitude. By taking the rms value of the table frequency variation, we cannot hope to get lower than $\delta f \gtrsim 1/\sqrt{2} \times 2 \times 10^{-4}$ Hz $= 1.4 \times 10^{-4}$ Hz. This corresponds to a rim acceleration of

$$\left.\frac{a}{g}\right|_{\text{ripple, rms}} = 4 \times 0.07 \text{ Hz} \times 1.4 \times 10^{-4} = 40 \text{ μg}. \tag{52}$$

This limit is quickly reached and indeed, all the measurements show an rms value from 35 μg to 45 μg.

From a harmonic analysis of one revolution, we might estimate that the noise will decrease as the square root of the number of pairs of points taken. Thus, for 1000 points, we might expect

$$\begin{aligned} F_{\text{noise}} &\gtrsim 1.4 \times 10^{-4}/(\sqrt{1000/2}) \\ &\gtrsim 6.3 \times 10^{-6} \text{ Hz}. \end{aligned}$$

At 0.07 Hz, this corresponds to

$$\left.\frac{a}{g}\right|_{\text{harmonic analysis limit = 1.7 μg}} = 4 \times 0.07 \text{ Hz} \times 6.3 \times 10^{-6} \text{ Hz} = 1.7 \times 10^{-6}. \tag{53}$$

This is very close to the actual spread in measured values of the table acceleration for the driven table, as shown in Fig. 23.

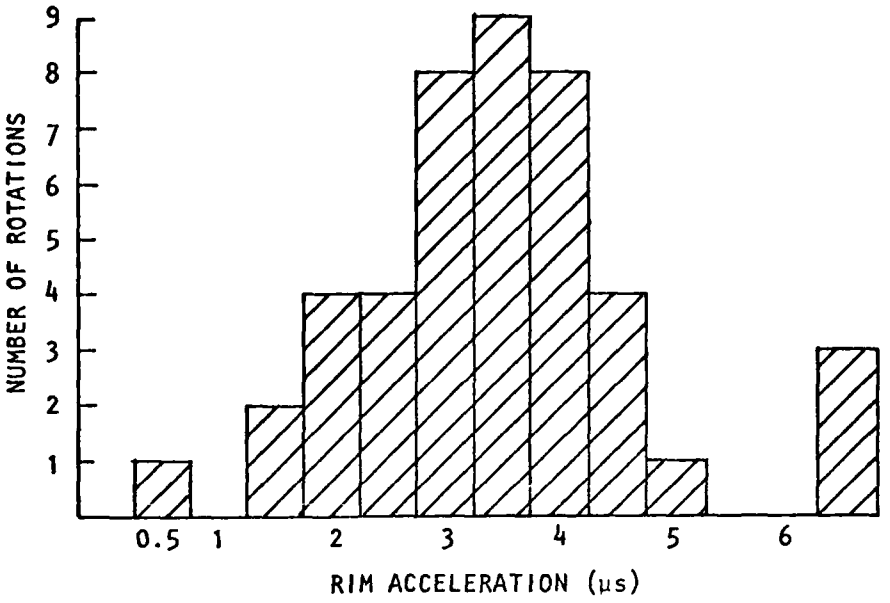

Fig. 23. Histogram of the measured rim acceleration amplitudes for a good balance comprising 44 different rotations. The 1 σ distribution is very close to the expected spread of ±1.7 μg, based on statistical noise due to the f/v converter ripple and limited measuring time.

A program has been written, labeled BALEN 2, outlined in Fig. 24, which takes up to 2000 speed measurements per rotation. A least squares fit is done to find the start frequency and the constant acceleration. This best straight line is subtracted off from the data, leaving the residual variation. A sine and cosine of the various rotation frequency harmonics are fitted to this residual. The starting frequency, the constant acceleration, the average frequency, the rms variation, and the harmonic amplitudes are then printed out. The residual speed variation is plotted on a strip chart

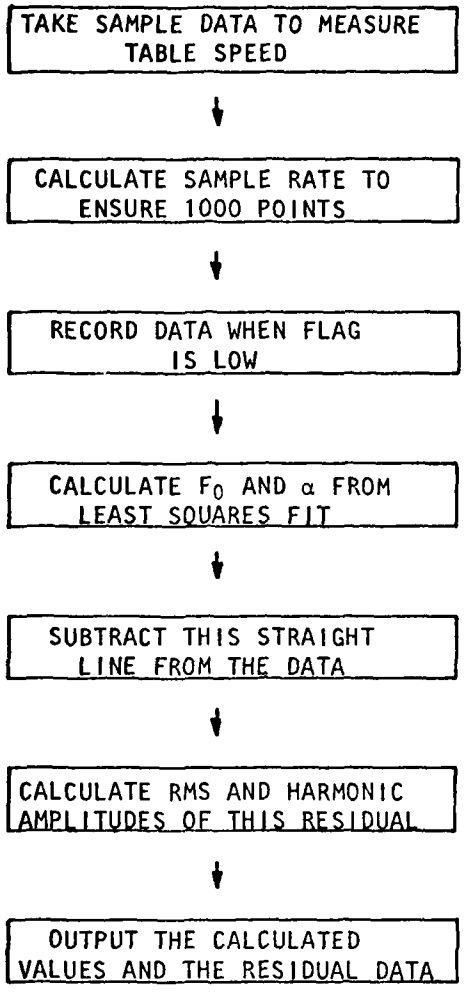

Fig. 24. Block diagram of the program BALEN2.

recorder via one of the D/A channels which controls the plotter. A sample of the data is shown in Fig. 25. A fundamental limitation in speed stability is set by the stability of the motor. The motor speed servo has similar characteristics loaded and unloaded. In Fig. 26 we show the frequency variation of the motor's armature over a long period, with its noise spectrum. At 0.07 Hz, the typical noise within a bandwidth of 1/512 (0.5 Hz) is approximately $\beta = 10^{-5}$. This corresponds to a stability in a bandwidth of 1/512 (0.07 Hz) of $\beta = 1.5 \times 10^{-6}$ and an acceleration of

$$\left.\frac{a}{g}\right|_{\text{motor stability} = 0.03\ \mu g} = 4 \times (0.07\ \text{Hz})^2 \times 1.5 \times 10^{-6}. \tag{54}$$

A summary of the noise sources and their limitations is shown in Table 1.

Balancing the Table

Balancing the table is accomplished in four stages

(1) Balancing without the shaft, then aligning the shaft's axis with the rotation axis.

(2) Alignment of the radial bearing to minimize rim acceleration.

(3) Matching of the tensions in the coupling springs.

(4) Weight balance of the rotating, driven table.

Initially, the balance weights were moved about the circumference, the table was spun up by hand, and freely slowed down. The acceleration was then measured using BALEN2. Figure 27 shows what the actual speed was with the output from BALEN2 for this and two other trials, with different loading. By this method, the rim acceleration was reduced to 10 μg. The shaft was then aligned to within 5 mil of the rotation axis. Such a

```
RUN

BALEN2  15-SEP-79  BASIC V01-05

THE TEST AVERAGE FREQUENCY IS  .077297
 WAITING FOR THE TRIG PULSE
GOT TRIG, TAKING DATA
 .077297         129          100          .129371      25.8742
 0               701          619
 1               701          619
 2               701          619
 3               699          619
 4               698          619
 5               698          619
 6               702          619
 7               700          619
 8               700          619
 9               699          619
 10              697          619
 THERE ARE  129  DATA POINTS TAKEN

 THE EST. AND CALC. STARTING FREQ. ARE  .0701  .0702807
 THE EST. AND CALC. AVERAGE FREQ. ARE   .0679  .0679752
 THE EST. AND CALC. ACCEL. ARE -2.98760E-04 -2.78458E-04
 THE RMS DEVIATION IS  1.81713E-04
 THE ACCELERATION PRODUCT IS  1.23520E-05

HARMONIC     SINE           COSINE         AMPLITUDE      PHASE ANGLE-DEGR
EES
 1           8.20610E-06    -4.82432E-05   4.89361E-05    80.3462
 2           -1.83361E-05   -2.35428E-06   1.84866E-05    172.686
 3           -1.15095E-05   -1.17742E-06   1.15696E-05    174.161
 4           1.65118E-05    -1.01953E-05   1.94057E-05    31.6918
 5           -2.56250E-05   6.10298E-06    2.63417E-05    13.394
 6           6.14591E-06    4.02357E-06    7.34584E-06    146.79
 7           -1.01111E-05   5.40324E-06    1.14643E-05    28.1176
 8           -2.15718E-05  -1.83151E-05    2.82981E-05    139.669
 9           4.48049E-06    2.31539E-05    2.35834E-05    100.952
 10          -8.42842E-06   6.81099E-06    1.08364E-05    38.9401
 1           3.32644E-06
 2           1.25663E-06
 3           7.86446E-07
 4           1.31911E-06
 5           1.79058E-06
 6           4.99335E-07
 7           7.79285E-07
 8           1.92357E-06
 9           1.60308E-06
 10          7.36607E-07
```

Rim acceleration, in g's

Fig. 25. Sample output from BALEN2 program showing the format of the result.

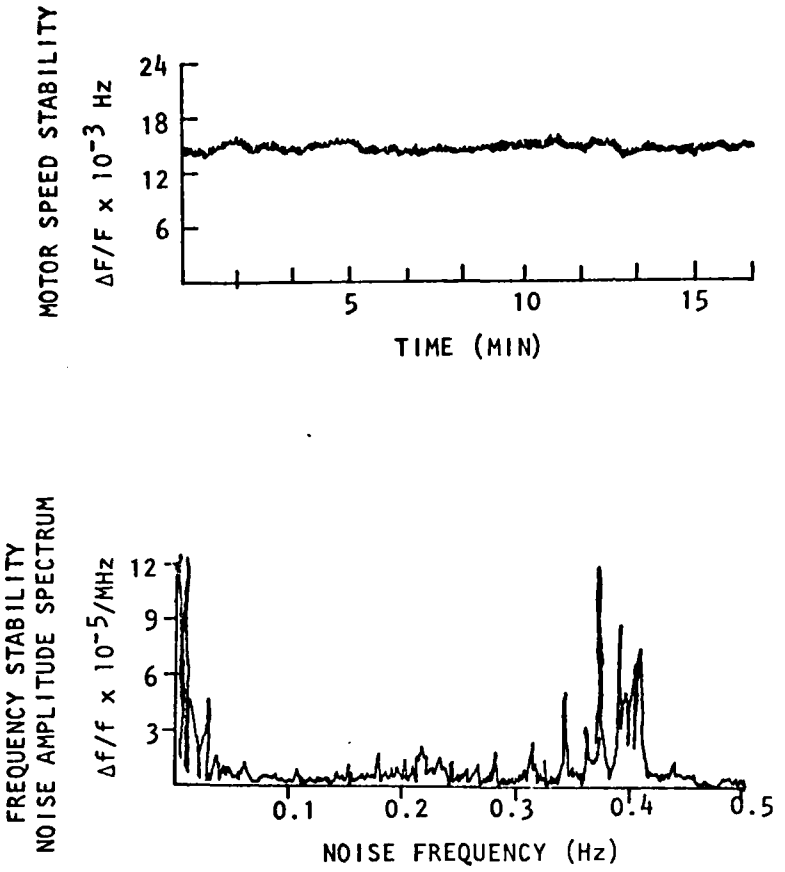

Fig. 26. Fractional speed variation of the drive motor, unloaded. (Top) In parts per 10^3 over 15 min. (Bottom) The FFT noise spectrum of this behavior. The peaks at 0.4 Hz are due to aliasing of the 200 Hz signal from the motor and the 1 Hz sample rate of the A/D converter. The vertical scale is fractional stability per a bandwidth of 1/512 (0.5 Hz).

Table 1. Noise Sources of Frequency Variation Limits and Stabilities for F = 0.07 Hz and the Expected Limit This Imposes on the Measurement of the Acceleration.

$$\frac{a}{g} = 4 \times F \times \delta F$$

$$\frac{a}{g} = 4 \times F^2 \times \beta; \qquad \beta = \frac{\delta F}{F}$$

$$\frac{a}{g} = 2 \times 10^{-2} \times \beta; \qquad F = 0.07 \text{ Hz}$$

Source	F (Hz)		$\frac{a}{g}$ (μg)
f/v stability		10^{-6}	0.02
Drive motor stability		1.5×10^{-6}	0.03
rms amplitude of ripple in f/v	1.4×10^{-4}	2×10^{-3}	40
Harmonic average of 1130/2 pairs of points	5.9×10^{-6}	8.4×10^{-5}	1.7
Glitch amplitude	2×10^{-4}	2.8×10^{-3}	56
Glitch amplitude averaged over 1 cycle	1×10^{-5}	1.4×10^{-4}	2.8
Missing 1 hole per rotation		1.3×10^{-3}	26

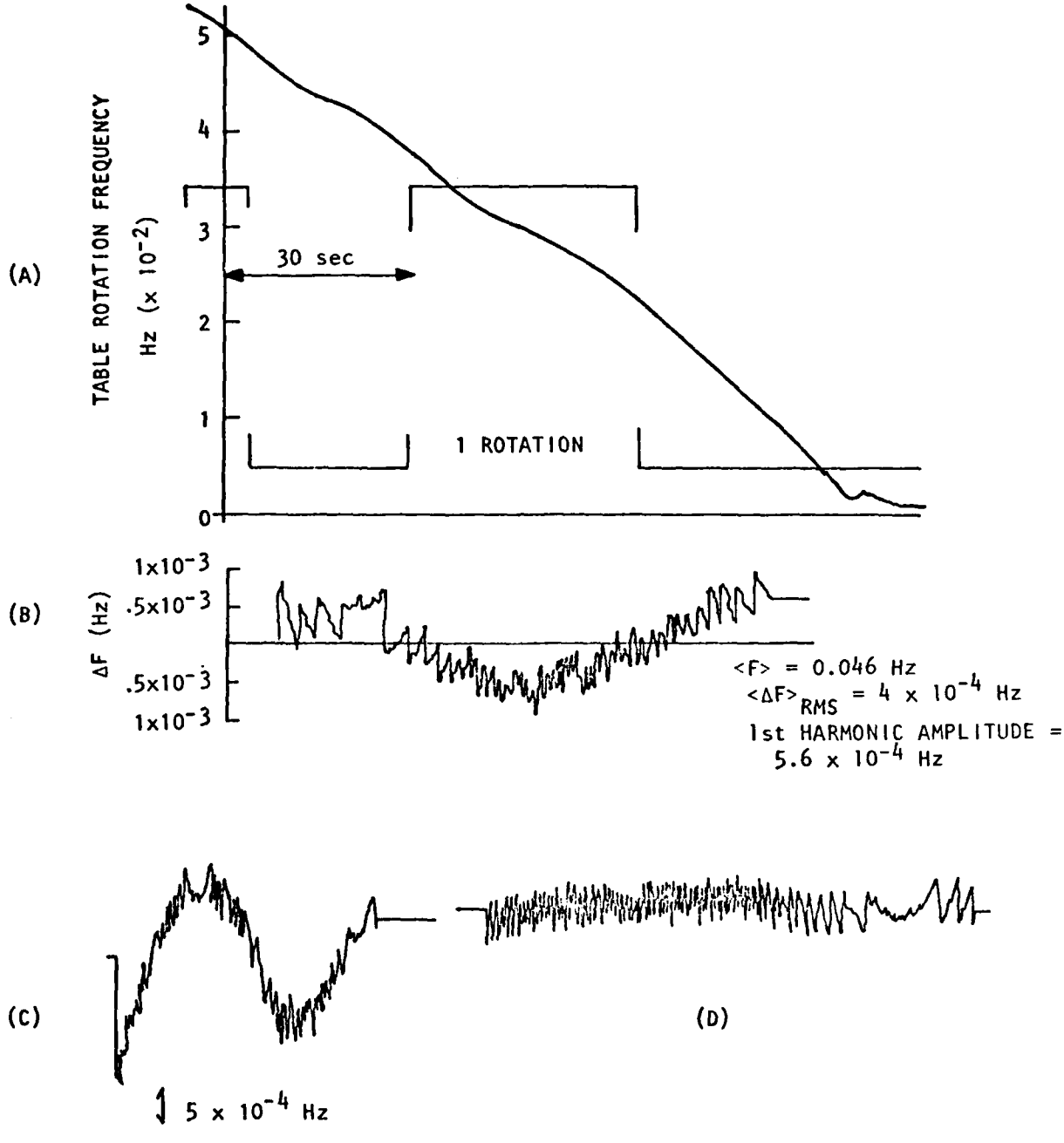

Fig. 27. Measurement of table speed. (a) Actual slow down of the table, with a flag superimposed, showing one rotation. (b) Reduced table speed with 10X greater vertical scale and different time scale. (c) Different plots of the reduced speed variation for differently balanced conditions. Note the magnitude of the ripple at $\pm 2 \times 10^{-4}$ Hz compared to the first harmonic amplitude. These data were taken before the drive motor was attached.

misalignment would cause an effective center of mass shift of a 3 ounce weight on the rim.

With the shaft in place, the radial bearing was aligned so as to produce smooth slow down. It is not clear what influence this alignment has on the table dynamics; however, the balance did change. The new balance conditions were easily found. A 20 lb weight was moved about the rim and the acceleration was measured as seen in Fig. 28. At the optimum rim position, different weights were tried to minimize the acceleration. With the best weight, the rim position was again optimized as shown in Fig. 29. After this point, the acceleration was reduced to 3 ± 2 μg. This residual acceleration might represent the instrumental limit of this particular speed sensor, set by the phase glitch where the tape joint comes together. The residual velocity variation of the table with this good balance is shown in Fig. 30.

We have pushed this simple speed sensor to its reasonable limits. The actual rim acceleration could be lower than 3 μg. Only a much improved method can answer this for sure. We are currently working on a new accelerometer system.

The Coupling Springs

An unexpected problem was noticed in the long-term frequency behavior of the table at low speeds, even with a good balance. Figure 31 shows the table speed after being changed from 0.07 Hz to 0.038 Hz. The apparent beating effect is obvious. The exact nature and cause are not clear. However, it seems in some way to be beating with the free oscillation of the table about the coupling springs. Monitoring the drive motor speed

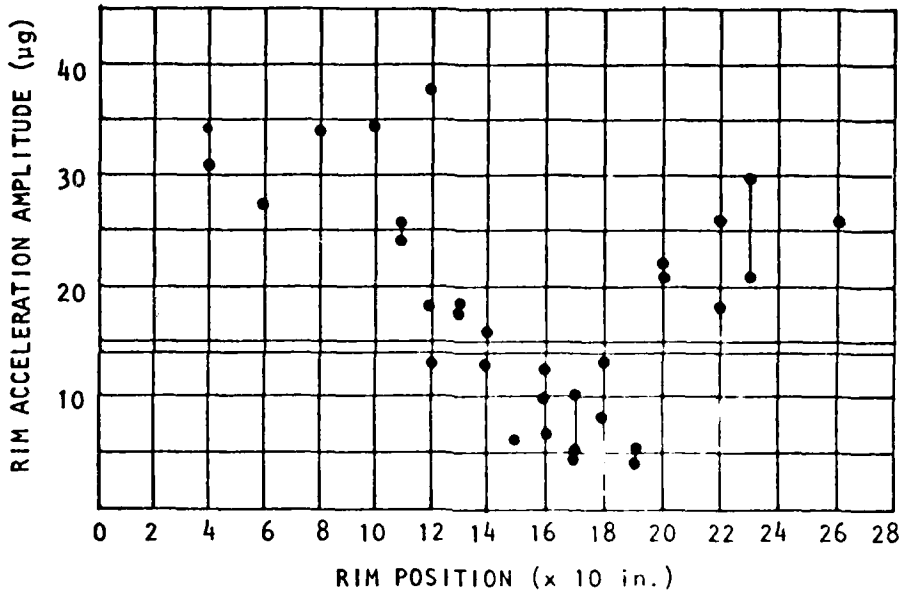

Fig. 28. Plot of the rim acceleration amplitude measured with BALEN2 at F = 0.07 Hz vs the position along the rim of a 20 lb weight.

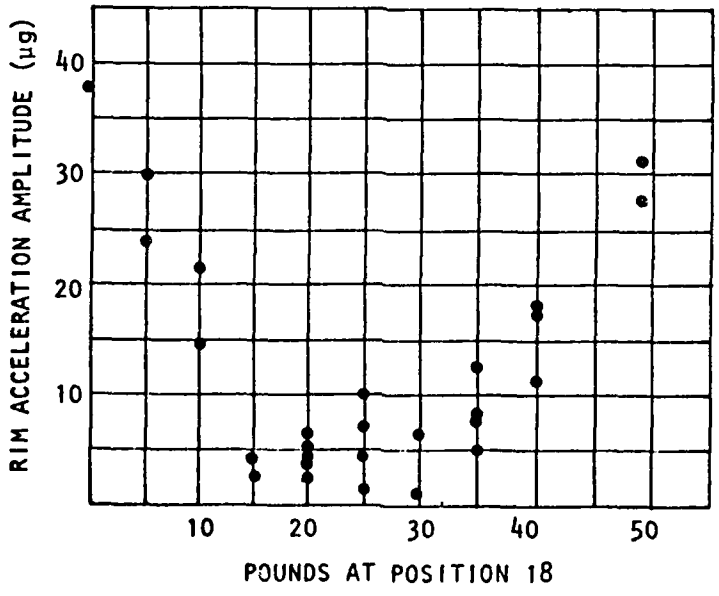

Fig. 29. Plot of the rim acceleration at F = 0.7 Hz vs the magnitude of a weight at position 18 along the rim.

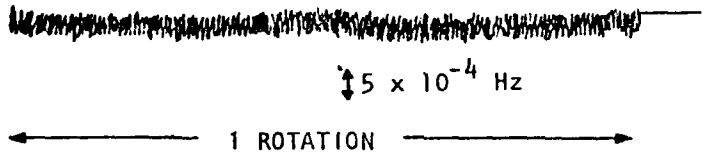

Fig. 30. Residual table behavior with a good balance at F = 0.07 Hz. The width of the line is 2×10^{-4} Hz, due to the ripple. Note the presence of the small phase glitch at a phase angle of 270° into the cycle.

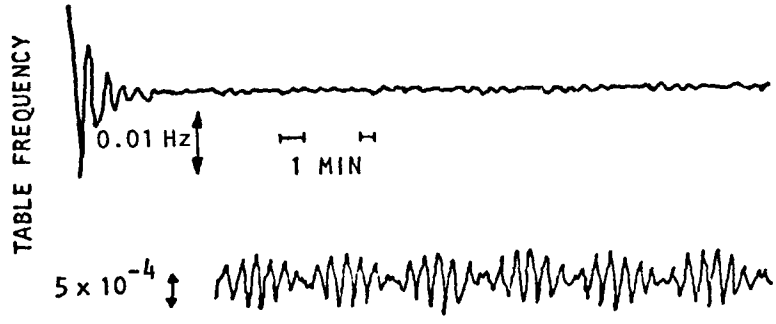

Fig. 31. Frequency behavior of the table after the speed was lowered showing clear beating. Lower curve is same velocity at 10 times more sensitivity.

shows that it retains its typical stability at 1 part in 10^6, and thus does not provide the coupling. The precise behavior of this beating depends on the balance condition, shown in Fig. 32. For more unbalance, the beating is worse. Decreasing the neutral position tension of the springs also strongly affects the beating, shown in Fig. 33. To reduce this effect, the springs were exchanged for two lengths of Tygon tubing, which makes very poor Hooke's law springs. Apparently, the balance of the tension in the two arms is critical. We show in Fig. 34 the effect on the table speed of a good match and a poor match. All the data reported here were taken with well matched Tygon tubing couplers. Figure 35 shows the final behavior of the table well balanced, with these Tygon tubing springs.

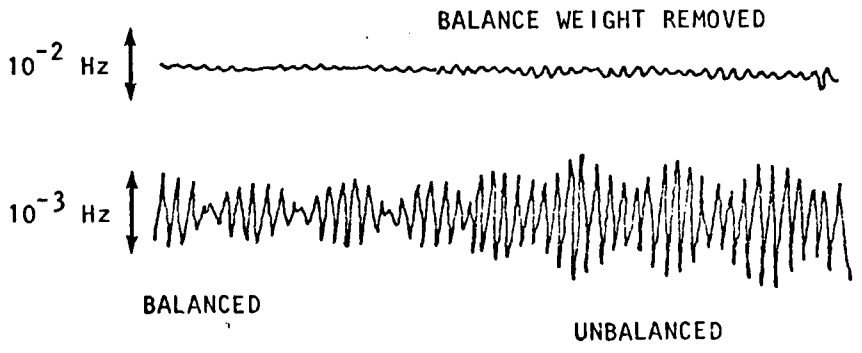

Fig. 32. Table frequency behavior at low speeds showing affect on the beating of an unbalance. The 25 lb balance weight was removed, increasing the beat amplitude.

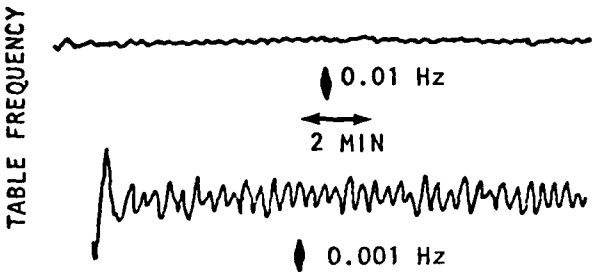

Fig. 33. Effect on table motion of relaxing the neutral position tension of the springs. The beating has decreased, but the first harmonic acceleration has increased.

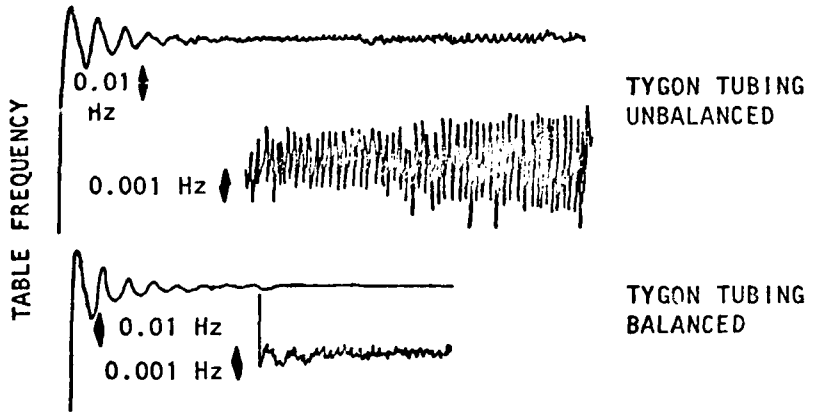

Fig. 34. Table frequency at F = 0.07 Hz. (Top) With Tygon tubing springs, not well matched for equal tension. Note no beating, but large acceleration. (Bottom) After tubing was removed, readjusted, and then replaced, showing very low acceleration. The residual peak in the 10X scale reading is part phase glitch and part chart recorder response.

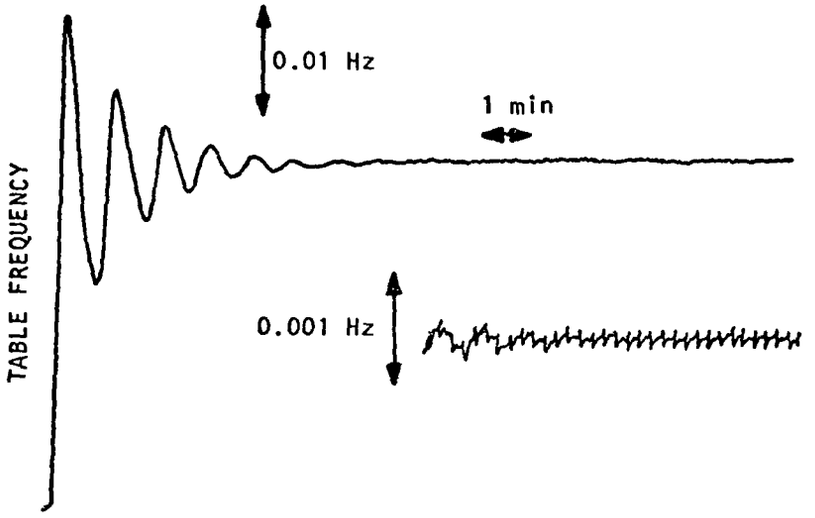

Fig. 35. Final behavior of the table showing the transient change and steady motion for long time period. This acceleration is 3 μg ± 2 μg which may be due only to the phase glitch apparent in the 10X scale.

EXPECTATIONS FOR THE SECOND ORDER EXPERIMENT

The current periodic rim acceleration of the table is a = 3 μg. This corresponds to an effective frequency variation in the lasers of 18 Hz. By optimizing the previously described parameters, we might further reduce this by a factor of 5 to 10. We expect the final frequency variation due to acceleration to be ≃ ±1 Hz. This limit is much below the inherent expected noise level of 3.5 Hz for a 1 sec average.

We have designed a very efficient accelerometer that also monitors tilt of the rotation axis. Our sensitivity is 10 μV/μg. By simultaneously monitoring the acceleration we can subtract a scaled value from the PZT servo voltage and reduce the effective frequency shift by another factor of 100.

If we approach this limit and keep the mechanical vibrations on this order also, we will than have

$$\left(\frac{v}{c}\right)^2 \lesssim \frac{\Delta L}{L} = \frac{\Delta \nu}{\nu} = \frac{3.5\ \text{Hz}}{8 \times 10^{13}\ \text{Hz}} = 4 \times 10^{-14},$$

for one rotation. An average for 3 hr should yield

$$\left(\frac{v}{c}\right)^2 \lesssim 4 \times 10^{-16}.$$

By searching for sidereal variation we expect to reach

$$\left(\frac{v}{c}\right)^2 \lesssim 4 \times 10^{-18}.$$

A TEST FOR ANISOTROPY OF THE METHANE ABSORPTION FREQUENCY

The assumption we make that the absorption frequency of the methane molecule is isotropic can be tested also. In the laser cavity, the methane molecule sees a linearly polarized radiation field. The field induces a dipole moment along this direction. One might expect an anisotropy to show up related to a preferred axis in space and the induced dipole moment direction. With a polarization axis perpendicular to the table, there will be no change in spatial orientation as the table rotates. However, by rotating the laser 90^{o} the induced dipole moment axis will now sweep through an orientation of 360^{o} as the table rotates. By comparing the servo voltage for the two different orientations we will be able to set a limit on the anisotropy of the absorption frequency of the methane molecule at

$$\frac{\Delta\nu}{\nu} \lesssim 4 \times 10^{-18}.$$

We could do this measurement directly by comparing the output frequency of two lasers with their polarization axes 90^{o} to each other. This would be a useful measurement for setting absolute frequency standards.

CONCLUSION

Our current limitation for a first order upper limit to the anisotropy in the speed of light is $v/c \lesssim 6 \times 10^{-3}$. This was limited by mechanical problems with the rotating table and frequency instabilities of the lasers. We have since removed all mechanical problems of the table and have increased the rotation frequency of the table by a factor of 30. We have designed and are currently building new lasers. With our new low noise detectors and electronics, which have recently been tested and are available, we expect to have over 300 times better frequency stability. This new system should yield an upper limit on v/c of approximately less than 10^{-6} for one rotation, 10^{-8} for 3 hr of data taking, and 10^{-10} for many days of data taking.

The current upper limit of the second order experiment is $(v/c)^2 \lesssim 10^{-11}$. This was limited by uncontrolled acceleration of the table. We have decreased this effect by a factor of 80 and with currently available accelerometers will be able to set this noise below the frequency noise limit of the lasers. We expect this experiment to yield an upper limit to $(v/c)^2$ of approximately less than 4×10^{-14} for one rotation, 4×10^{-16} for 3 hr of data taking, and 4×10^{-18} for many days of data taking.

REFERENCES

1. A. A. Michelson, Am. J. Sci. 22, 120 (1881).

2. V. C. Rubin, W. K. Ford, N. Thonnard, M. S. Roberts, and J. A. Graham, Astron. J. 81, 687 (1976).

3. G. F. Snoot, M. V. Gorenstein, and R. A. Muller, Phys. Rev. Lett. 39, 898 (1977).

4. V. W. Hughes, H. G. Robinson, and V. Beltran-Lopez, Phys. Rev. Lett. 4, 342 (1960).

5. R. W. P. Drever, Phil. Mag. 6, 683 (1961).

6. A. Brillet and J. L. Hall, Phys. Rev. Lett. 42, 459 (1979).

7. E. Bogatin and J. Small, "Electromagnetic anisotropy," project review for AFOSR contract F49620-77-C-0021, Optical Sciences Center, University of Arizona, Tucson, Arizona, January 18, 1979.

8. E. W. Silvertooth, Appl. Opt. 15, 1100 (1976).

9. Roy Gibbson, Judson IR Industries, Inc., Waltham, Massachusetts, private communication, 1979.

10. V. G. Joos, Ann. Physik 7, 385 (1930).

11. J. S. Jaseja, A. Javan, J. Murray and C. H. Townes, Phys. Rev. 133, A1221 (1964).